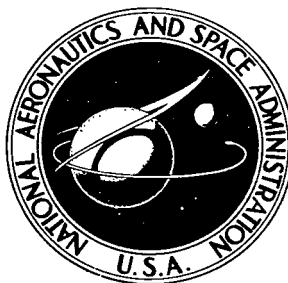


NASA TECHNICAL NOTE



NASA TN D-4661

NASA TN D-4661



LOAN COPY: RETURN TO
AFWL (WLIL-2)
KIRTLAND AFB, N MEX

**EFFECT OF
10²⁰-NEUTRON-PER-SQUARE-CENTIMETER
IRRADIATION ON EMBRITTLEMENT
OF POLYCRYSTALLINE TUNGSTEN**

by Charles L. Younger and Gilbert N. Wrights

Lewis Research Center

Cleveland, Ohio





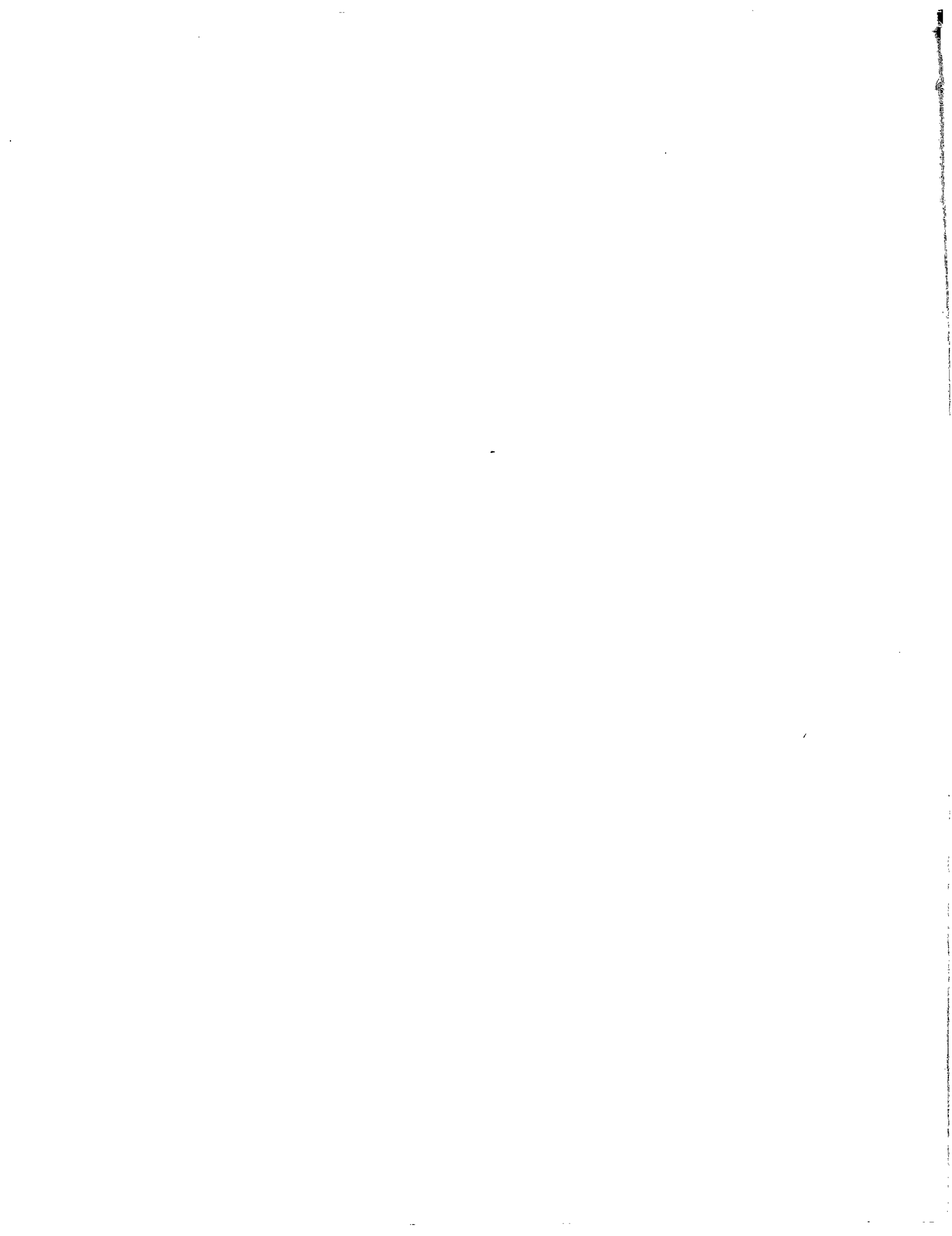
EFFECT OF 10^{20} -NEUTRON-PER-SQUARE-CENTIMETER IRRADIATION
ON EMBRITTLEMENT OF POLYCRYSTALLINE TUNGSTEN

By Charles L. Younger and Gilbert N. Wrights

Lewis Research Center
Cleveland, Ohio

NATIONAL AERONAUTICS AND SPACE ADMINISTRATION

For sale by the Clearinghouse for Federal Scientific and Technical Information
Springfield, Virginia 22151 - CFSTI price \$3.00



CONTENTS

	Page
SUMMARY	1
INTRODUCTION	2
TEST MATERIAL	3
IRRADIATION	7
TEST APPARATUS AND PROCEDURES	10
Tensile Tests	10
Bend Tests	12
Metallography	13
Dimensional Measurements	14
Density Determinations	14
Electrical Resistivity Determinations	15
TEST RESULTS	17
Neutron Flux	17
Tensile Properties	18
Bend Properties	23
Dimensions	27
Density	27
Electrical Resistivity	29
DISCUSSION OF TEST RESULTS	31
Surface Condition	31
Impurities	33
Carbon	34
Oxygen	34
Miscellaneous	34
Rhenium	35
Metallurgical Defects	36
SUMMARY OF RESULTS AND CONCLUSIONS	38
APPENDIXES	
A - ACTIVATION EQUATION FOR CALCULATING THERMAL NEUTRON FLUX	41
B - ACTIVATION EQUATION FOR CALCULATING FAST NEUTRON FLUX	42
REFERENCES	44

EFFECT OF 10^{20} -NEUTRON-PER-SQUARE-CENTIMETER IRRADIATION ON EMBRITTLEMENT OF POLYCRYSTALLINE TUNGSTEN

by Charles L. Younger and Gilbert N. Wrights

Lewis Research Center

SUMMARY

The effect of reactor irradiation on embrittlement of polycrystalline tungsten has been investigated by comparing ductile-to-brittle transition behavior of unirradiated and irradiated material. Tensile tests conducted in the range 300° to 700° F (422 to 644 K) were used to determine ductile-to-brittle transition behavior. Bend tests, conducted at room temperature, provided additional data for investigating irradiation embrittlement.

Tensile and bend test results show that recrystallized tungsten irradiated with 1×10^{20} fast neutrons per square centimeter is severely embrittled. The ductile-to-brittle transition temperature for the irradiated material increased by at least 300° F (167 K) and was accompanied by an increase in the temperature-dependent yield point stress and decreases in the tensile fracture and extreme fiber bending stresses. The embrittlement appears to be a result of factors which decrease grain boundary strength and inhibit transgranular fracture.

The change due to irradiation was also determined for test specimen dimensions, density, and electrical resistivity. Dimensional and density changes were small, but the electrical resistivity increased linearly with increasing irradiation. The change in electrical resistivity at the highest irradiation exposure was 87 percent.

Based on analysis of the test data, it may be concluded that irradiation of unalloyed, polycrystalline tungsten with 10^{20} fast neutrons per square centimeter and 10^{21} thermal neutrons per square centimeter produces a very brittle tungsten - 1-percent-rhenium alloy. The strength of this alloy is greater than that of the starting material, but because of the presence of irradiation-induced point defects, dislocation loops, and various defect clusters, the grain boundary strength of the alloy is lower than the starting material.

INTRODUCTION

Although unalloyed tungsten exhibits desirable engineering properties at elevated temperatures, the metal is brittle at room temperature. The transition from ductile behavior to brittle behavior is quite pronounced and occurs at about 500 K (e. g., ref. 1). This pronounced ductile-to-brittle transition behavior provides a useful tool for studying the effect of nuclear irradiation on the metal.

Following exposure to nuclear irradiation at or near room temperature, metallic materials normally exhibit an increase in strength and a decrease in ductility. This effect also tends to increase the temperature for ductile-to-brittle transition behavior.

The only known studies of the effect of irradiation on the ductile-to-brittle transition behavior of tungsten have been reported by Makin and Gillies (ref. 2). These experimenters conducted bend tests at various temperatures using 0.040-inch- (1.0-mm-) diameter wire specimens of fully recrystallized tungsten. Test results show that irradiation with 5×10^{19} neutrons per square centimeter changed the ductile-to-brittle transition temperature from 393 to 401 K, an increase of only 8 K.

In addition to the bend - transition-temperature studies, Makin and Gillies conducted tensile tests at 373 and 473 K with the same test material. Test specimens were again 0.040-inch- (1.0-mm-) diameter wires. Test results at 373 K showed the metal was brittle with no evidence of yielding nor ductility for both unirradiated and irradiated conditions. However, the irradiation to 5×10^{19} fast neutrons per square centimeter did result in an increase of about 11 percent in the tensile fracture strength. Similar tests conducted at a 473 K test temperature showed the metal to be ductile for both unirradiated and irradiated conditions, with the reduction of area and elongation being increased by the irradiation exposure. There were no significant differences in ultimate tensile strength, but the yield strength of the irradiated material decreased about 11 percent.

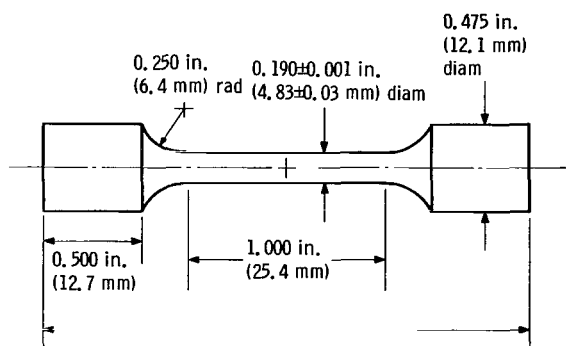
Sutton and Leeser (ref. 3) reported tensile test results for tungsten irradiated with 5×10^{19} fast¹ neutrons per square centimeter, and then tested at room temperature. Test specimens were 0.110-inch (2.8-mm) gage diameter and failed in a brittle manner for both unirradiated and irradiated conditions. The tensile fracture strength of irradiated material was reduced by 22 percent. The initial condition of the material was not reported. However, the unirradiated value for the tensile fracture strength was 145 500 to 160 000 psi (100 322 to 110 320 N/cm²) which suggests that the material was drawn and then stress relieved (e. g., refs. 4 to 7). These experimenters attributed the reduction in strength to be partly a result of the difficulty of alining the brittle specimens by remote control.

¹All fast flux values quoted in remainder of text are for neutron energy greater than 1 MeV unless otherwise noted.

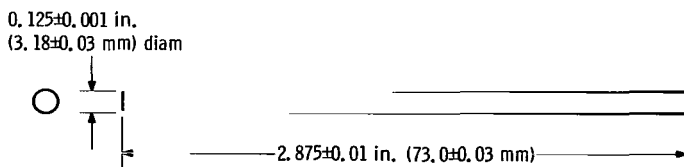
Since wire specimens are not necessarily representative of tungsten material for structural applications (ref. 8) and in view of the reduction in strength reported in the literature, an experimental investigation of the effect of reactor irradiation on embrittlement of polycrystalline tungsten rod was undertaken. Tensile and bend tests were performed in the investigation for the purpose of determining the effect of reactor irradiation on embrittlement. Physical property measurements, dimensions, density, and electrical resistivity were also included in the test program for comparison with results of other investigations.

TEST MATERIAL

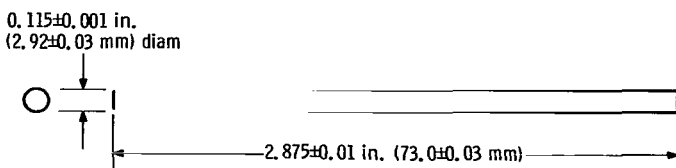
Commercially pure sintered then swaged tungsten rod in two stock sizes, 0.500-inch (12.7-mm) and 0.125-inch (3.2-mm) diameters, was obtained from a commercial



(a) Tensile specimen (electropolished gage length).



(b) Bend specimen (unpolished).

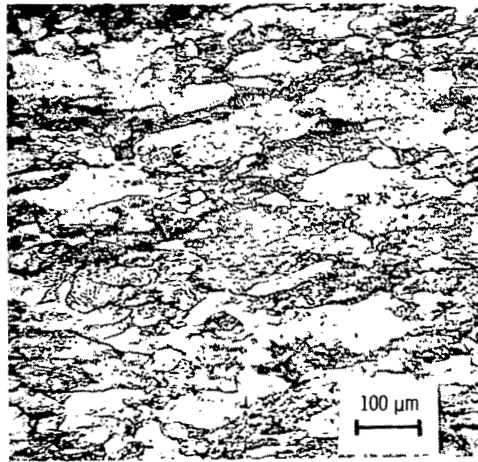


(c) Bend specimen (electropolished).

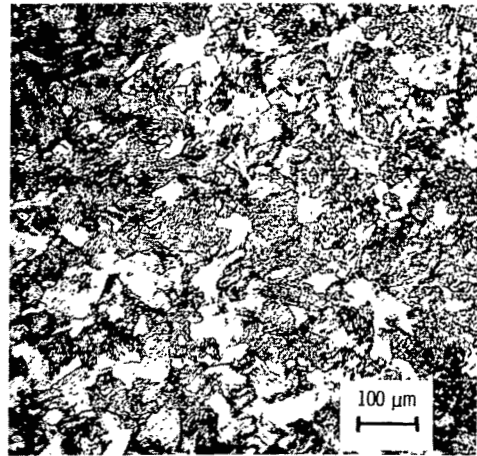
Figure 1. - Tungsten test specimens.

supplier for use in this investigation. Spectrographic and chemical analysis of the stock materials are shown in table I.

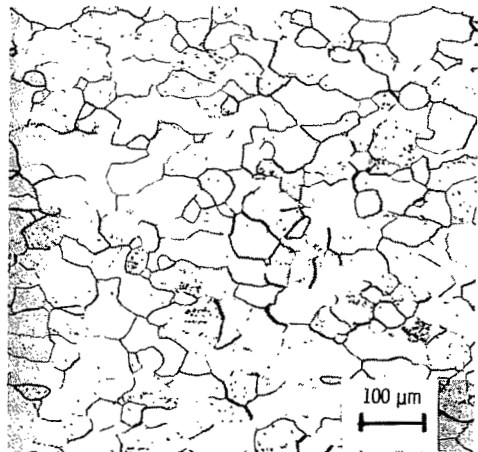
Tensile test specimens (fig. 1(a)) were prepared from the 0.500-inch- (12.7-mm-) diameter rod stock. Test specimens were first ground to the specified dimensions and then vacuum annealed at 3500^o F (2200 K) for 1 hour to eliminate the effect of prior cold working. Finally, each test specimen gage length and gage-length-to-buttonhead fillet was electropolished in accordance with procedures and apparatus previously reported (ref. 9). The electropolishing treatment reduced the test specimen diameter from



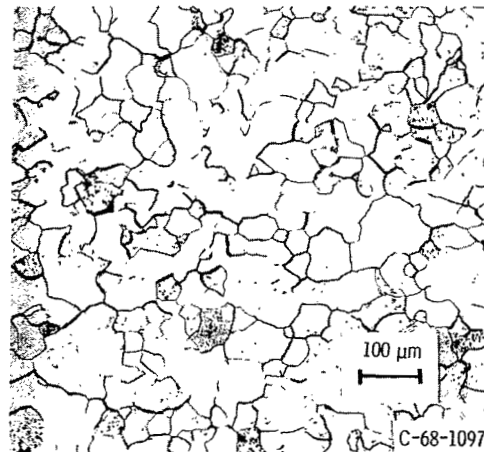
(a) As-received, longitudinal direction.



(b) As-received, transverse direction.



(c) Annealed, longitudinal direction.

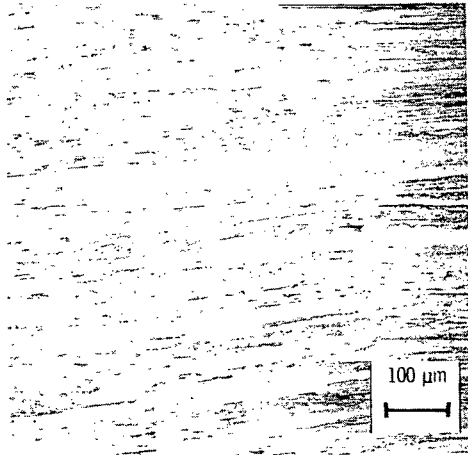


(d) Annealed, transverse direction.

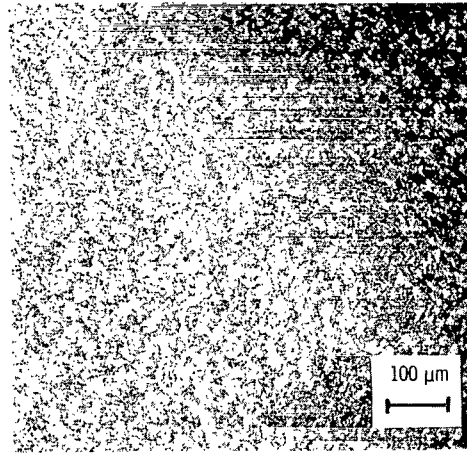
Figure 2. - Photomicrographs of as-received and annealed tensile specimens. Etched with 75 grams of potassium ferricyanide ($K_3Fe(CN)_6$) and 20 grams of sodium hydroxide in 500 cubic centimeters of water. X75.

0.200 inch (5.1 mm) to 0.190 inch (4.8 mm) and permitted dimensional tolerances to be held within ± 0.0005 inch (± 0.01 mm).

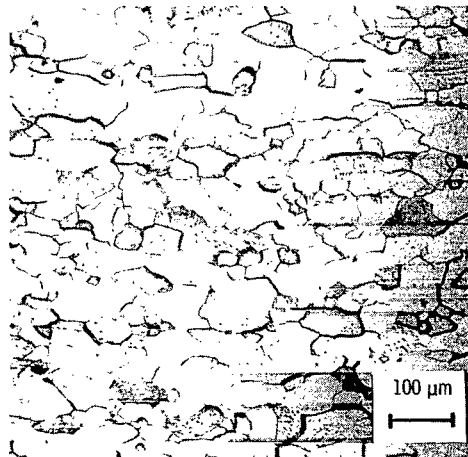
Bend test specimens (figs. 1(b) and (c)) were prepared from the 0.125-inch- (3.2-mm-) diameter rod stock. Test specimens were first cut to the specified lengths and then vacuum annealed at 3500° F (2200 K) for 30 minutes. Most test specimens were then reduced to a 0.115-inch (2.9-mm) diameter by electropolishing; however, a number of test specimens were retained in the as-annealed surface condition with a diameter of 0.125 inch (3.2 mm).



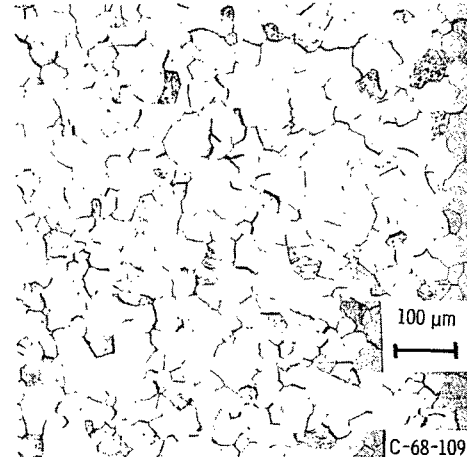
(a) As-received, longitudinal direction.



(b) As-received, transverse direction.



(c) Annealed, longitudinal direction.



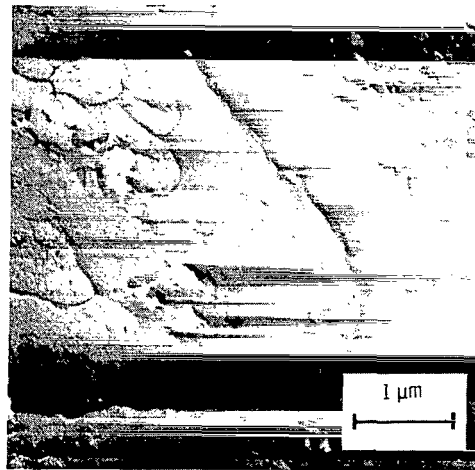
(d) Annealed, transverse direction.

Figure 3. - Photomicrographs of as-received and annealed bend specimens. Etched with 75 grams of potassium ferricyanide ($K_3Fe(CN)_6$) and 20 grams of sodium hydroxide in 500 cubic centimeters of water. X75.

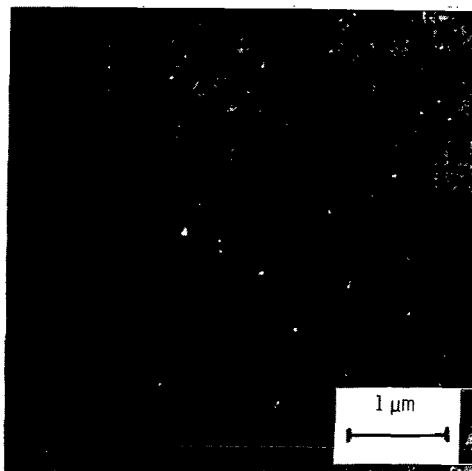
Photomicrographs (figs. 2 and 3) show that the annealing treatment produced an equiaxed grain of about the same size in both tensile and bend test specimens. For the tensile specimens, there is no apparent difference in grain structure in the longitudinal and transverse directions, but for the bend specimens, the grain is somewhat elongated in the swaging (longitudinal) direction. The improvement in surface finish by the electropolishing treatment is shown in the electron micrographs of figure 4.



(a) As-received, swaged, and ground.



(b) Annealed, 1/2 hr at 3500° F (2200 K).



C-68-1099

(c) Electropolished, surface reduction of 0.005 inch (0.11 mm).

Figure 4. - Electronmicrographs of as-received, annealed, and electropolished surfaces. Etched with 75 grams of potassium ferricyanide ($K_3Fe(CN)_6$) and 20 grams of sodium hydroxide in 500 cubic centimeters of water. X12 500.

IRRADIATION

Test specimens were irradiated in the NASA Plum Brook Reactor for a period of 269 hours. The maximum fast flux during irradiation was about 1.1×10^{14} neutrons per square centimeter per second. For irradiation, the test specimens were placed in an aluminum irradiation capsule (figs. 5 and 6) designed to fit the LA-7 position of the re-

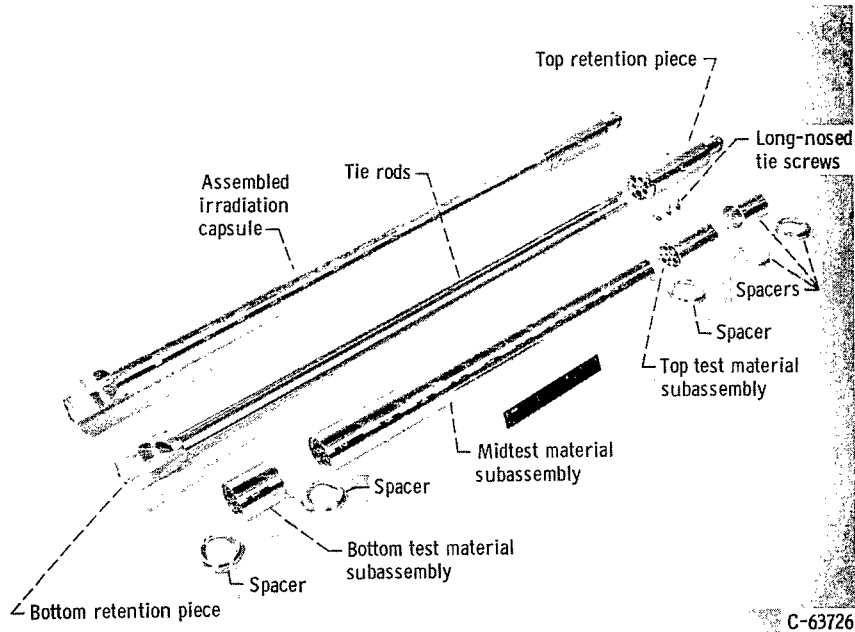


Figure 5. - Irradiation capsule assembly.

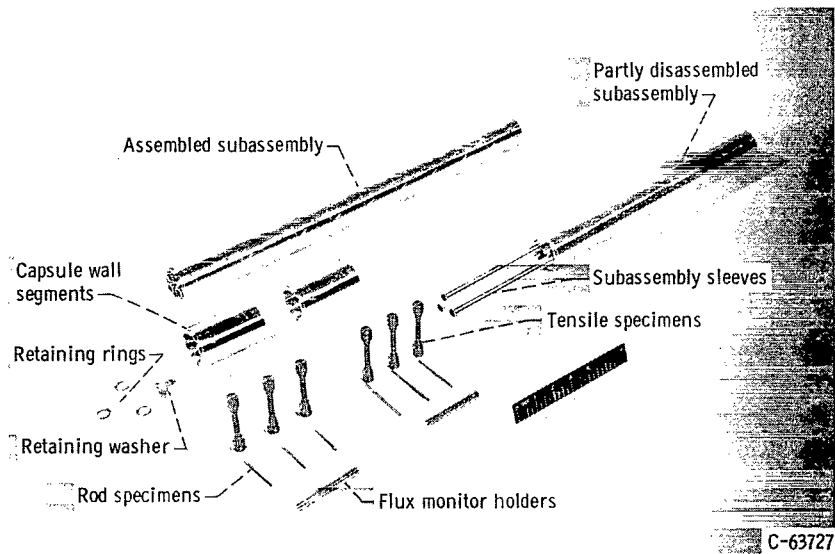


Figure 6. - Irradiation capsule subassembly.

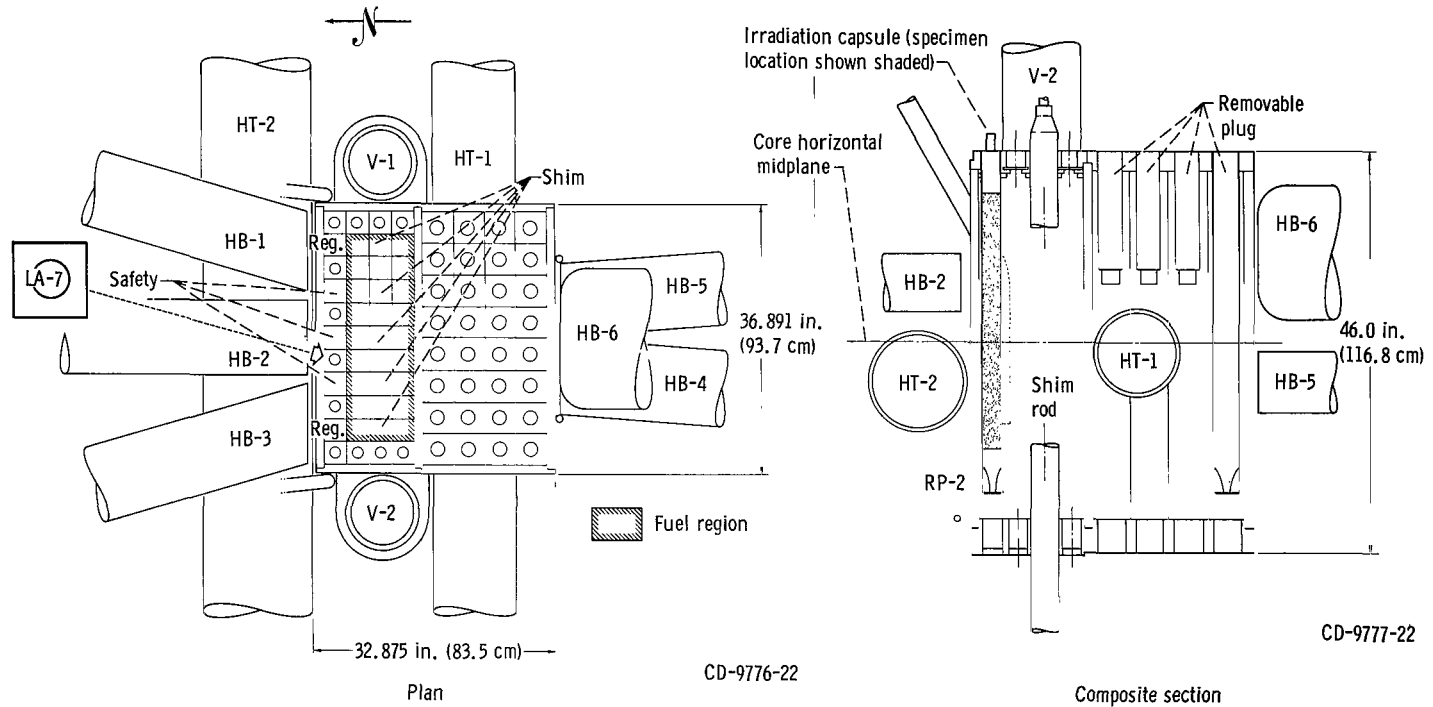
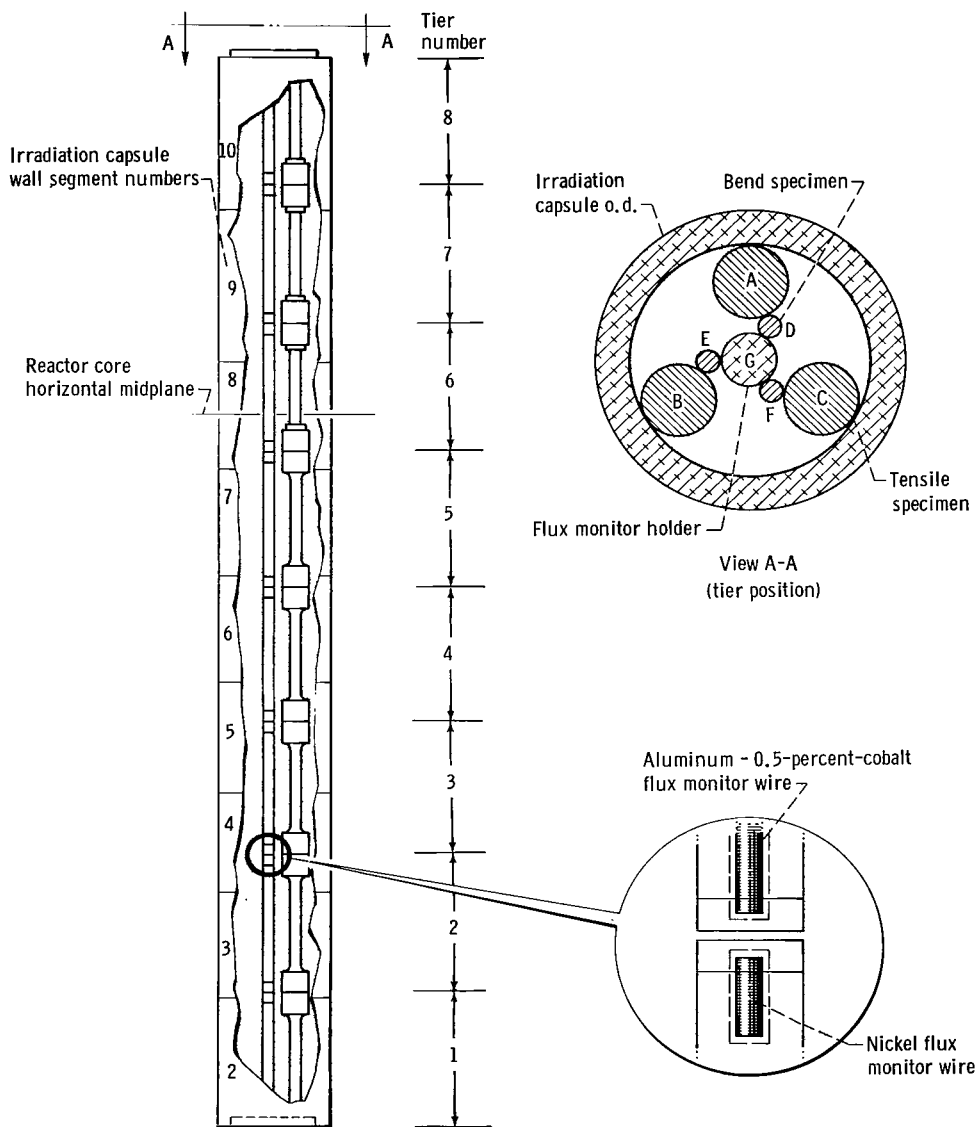


Figure 7. - NASA Plum Brook reactor core and irradiation test holes.

actor (fig. 7). This capsule is described in detail in reference 10. For irradiation purposes, the capsule provides a 30-inch (76-cm) length wherein test specimens and flux monitor holders are positioned in tiers (fig. 8). Each tier consists of three tensile specimens (positions A, B, and C) three bend specimens (positions D, E, and F), and a flux monitor holder (position G). For this investigation, tensile test specimens were located in positions A, B, and C of tiers 1 to 5. Bend test specimens occupied positions D, E, and F of tiers 6 to 8.



CD-9741

Figure 8. - Irradiation capsule loading scheme.

During irradiation, test specimens were cooled by reactor primary water flowing through the capsule at about 10 feet per second (3.3 m/sec). The specimen temperature was not monitored, but, based on a heat-transfer analysis using a computer program (TØSS, ref. 11) it was calculated to be less than 200^o F (366 K).

Following irradiation, the capsule assembly was removed from the reactor and stored for about 3 months prior to disassembly and specimen testing. Since the specimens were exposed to water during irradiation and storage, all surfaces were rubbed lightly prior to testing to remove any loose film or contaminants which might be adhering.

The neutron flux was determined by activation analysis of 0.030-inch- (0.8-mm-) diameter by 0.500-inch- (12.7-mm-) long wires irradiated in flux monitor holders along with the test specimens. Each flux monitor holder contained two wires, one aluminum - 0.5 percent cobalt and one 99.98 percent nickel. A detailed discussion of the neutron flux determination is presented in appendixes A and B.

TEST APPARATUS AND PROCEDURES

The investigation consisted of testing duplicate sets of unirradiated and irradiated polycrystalline tungsten tensile and bend specimens. Tensile tests, bend tests, metallography, dimensional measurements, density determinations, and electrical resistivity determinations were performed remotely in the NASA Plum Brook Reactor Facility hot laboratory (ref. 12). Measurements on the unirradiated and irradiated specimens were obtained by using the same test apparatus and test procedure in order that direct comparisons could be made.

Tensile Tests

Tensile tests were performed at 300^o, 400^o, 500^o, 600^o, and 700^o F (422, 477, 533, 589, and 644 K) on a 10 000-pound (44 500-N) tensile testing machine adapted to remote operation. A tubular testing furnace, hinged mounted on the frame of the test machine (fig. 9), was used for the elevated temperatures. To alleviate alignment problems, an axial loading tensile testing fixture (fig. 10) was also used. The loading fixture is a modification of an axial loading creep fixture (ref. 13) and employs the principle of axial loading through spherical balls positioned in line with the axis of the pull rod assembly.

Test specimens were brought to test temperature, soaked for 10 minutes at temperature, and then pulled to fracture at a constant crosshead speed of 0.2 inch per minute (5.1 mm/min). The furnace controller was calibrated by a thermocouple near, but not

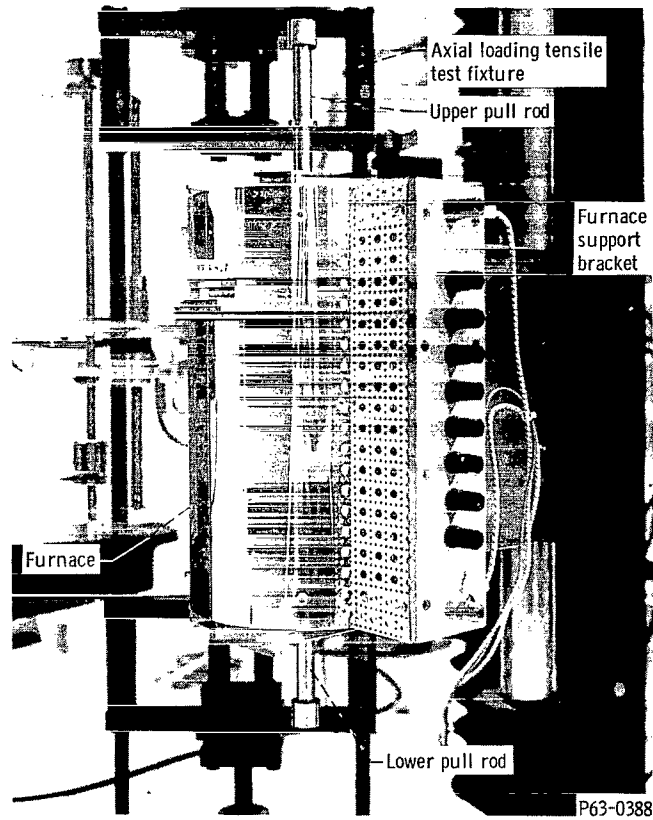


Figure 9. - Tensile testing furnace.

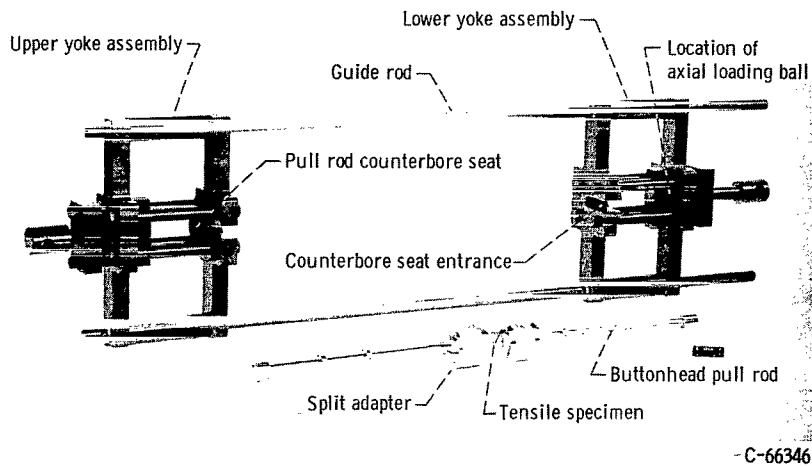


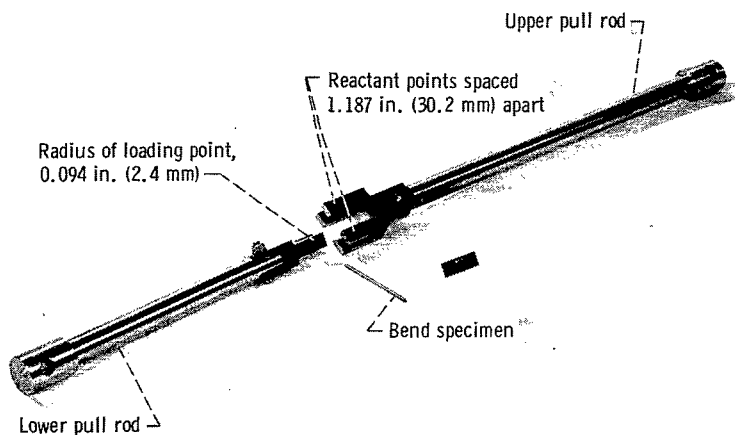
Figure 10. - Axial loading tensile testing fixture and pull rod assembly.

attached to, the gage section of the test specimen. Load-time curves were obtained autographically.

Following fracture, photographs were taken of each tensile test specimen. Longitudinal and cross-sectional views were taken at magnifications of 1 and 4, respectively. Unirradiated test specimens were photographed out-of-cell by conventional techniques. Irradiated test specimens were photographed in-cell with the assistance of a scanning periscope.

Bend Tests

Bend tests were performed at room temperature on the same machine as the tensile tests. The grips of the tensile machine were replaced with the fixture shown in figure 11. This fixture has two fixed reactant points separated by a span of 1.187 inches



C-65966

Figure 11. - Bend test fixture.

(30.2 mm) and a fixed loading point midway between the reactant points. The radius of the reactant and loading points is 0.094 inch (2.4 mm).

A small load, less than 1 pound force (4.45 N), was first applied to the test specimen for alinement and then the specimen was pulled to fracture at a constant crosshead speed of 0.02 inch per minute (0.51 mm/min). Load-time curves were plotted autographically. Extreme fiber stress was calculated from the flexure formula

$$f_b = \frac{M_y}{I}$$

where

f_b extreme fiber stress, N/cm^2

M applied bending moment, $cm-N$

y distance from neutral axis to extreme fiber, cm

I moment of inertia of cross section about its neutral axis, cm^4

Metallography

Tangential longitudinal photomicrographs were obtained of the fractured zone for each tensile and bend test condition. Appropriate sections were cut from the test specimens with a small water-cooled abrasive cutoff wheel. These sections were mounted in an epoxy, ground through four grits (220, 320, 400, and 600) and polished on a vibratory polisher. Etching was performed by swabbing with a solution of 75 grams of potassium ferricyanide ($K_3Fe(CN)_6$) and 20 grams of sodium hydroxide in 500 cubic centimeters of water for 4 seconds.

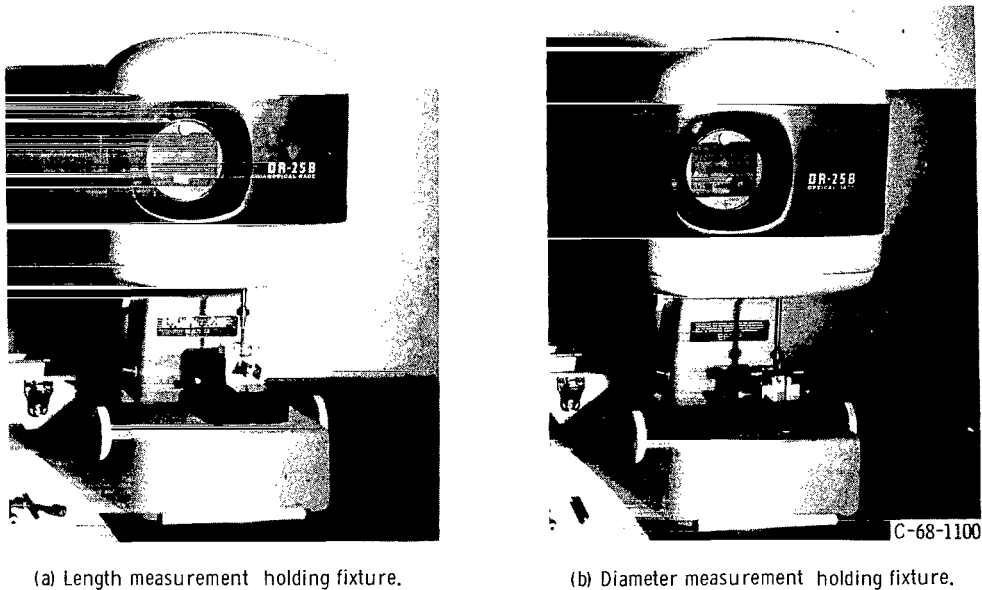


Figure 12. - Optical gage and test specimen holding fixtures.

Dimensional Measurements

An optical gage fitted with a flat 0.125-inch- (3.2-mm-) diameter tip was used for dimensional measurements on all test specimens. The specimen holding fixtures shown in figure 12 were employed for performing the measurements by remote techniques. Dimensional readings taken with this equipment are accurate to ± 0.00001 inch (± 0.00025 mm). For the irradiated specimens, dimensional measurements were made both before and after irradiation exposure.

Density Determinations

The density ω of each test specimen was determined by the hydrostatic method from the formula

$$\omega = \frac{W_a \omega_l}{W_a - W_l}$$

where

ω specimen density, g/cm^3

W_a specimen weight in air, g

W_l specimen weight in immersing fluid, g

ω_l immersing fluid density, g/cm^3

An accuracy of the order of 0.01 to 0.001 gram per cubic centimeter is obtainable by this method (ref. 14).

Specimen weight measurements were performed remotely on an analytical balance fitted with a specimen hanger and fluid tank, as shown in figure 13. The density of all test specimens for the unirradiated condition was determined by using distilled water with small additions of dioctyl sodium sulfosuccinate as the immersing fluid. The density of the test specimens following irradiation was determined by using reagent grade carbon tetrachloride as the immersing fluid. All density measurements were corrected to a reference temperature of 68°F (293 K).

Pre- and postirradiation volumes for the test specimens were determined by dividing the specimen weight in air by the calculated density of the specimen.

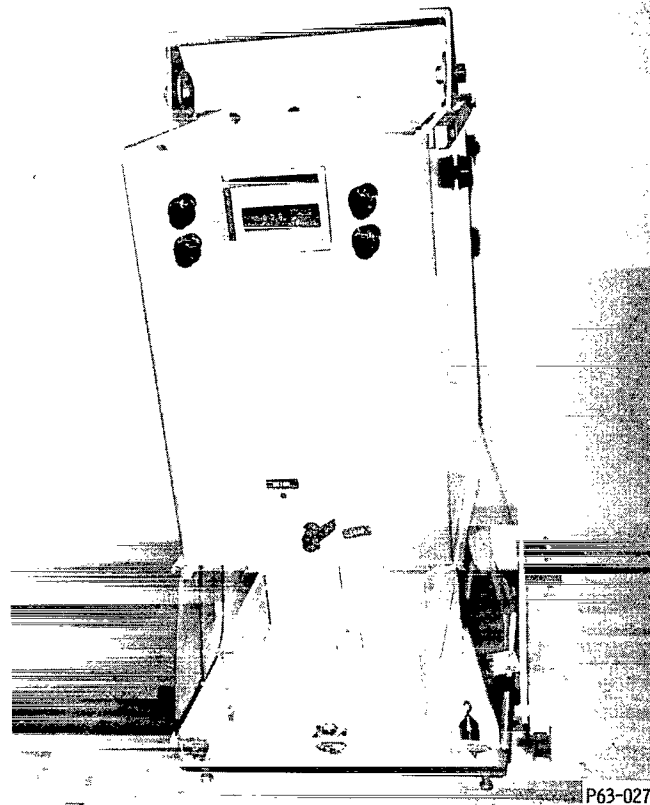


Figure 13. - Analytical balance.

Electrical Resistivity Determinations

Electrical resistivity, at a controlled temperature, was determined by the potential drop method from the formula

$$\rho = \frac{RA}{L}$$

where

ρ electrical resistivity, ohm-cm

R resistance, ohm

A specimen cross-sectional area, cm²

L resistance length, cm

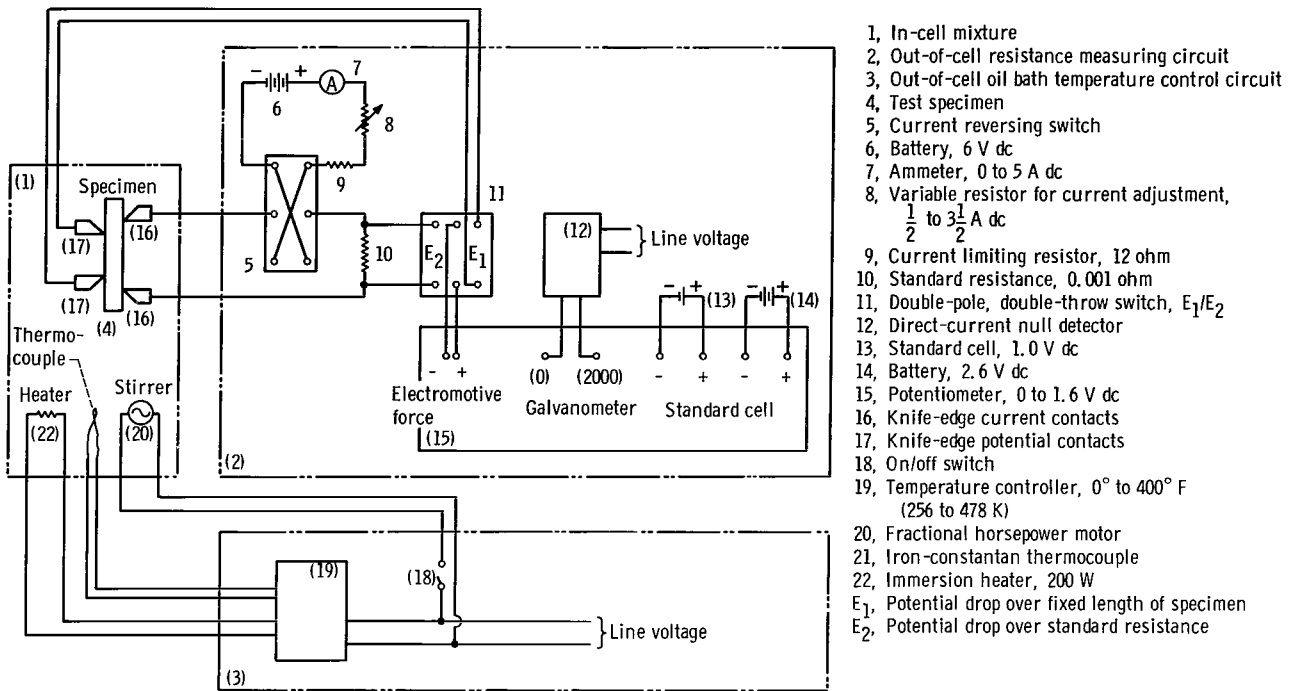
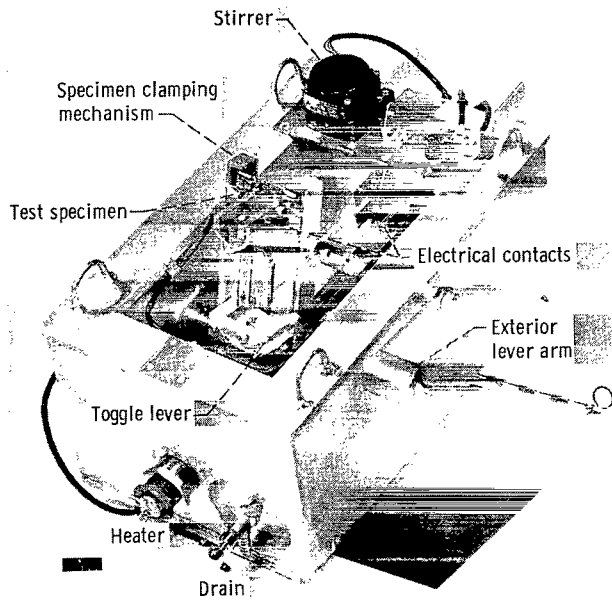


Figure 14. - Electrical resistivity measuring circuit.



C-65962

Figure 15. - In-cell fixture for electrical resistivity measurements.

The test technique employed was similar to that used by others (refs. 15 and 16). The circuit diagram for the test apparatus is shown schematically in figure 14. This apparatus consists essentially of two parts: an in-cell fixture for test specimen installation and an out-of-cell control and measuring console.

The in-cell fixture (fig. 15) was designed to accommodate both tensile and bend test specimens. The test specimen is first installed in the specimen clamping mechanism and then lowered, by the exterior lever arm, into an oil bath. The toggle lever is then moved to engage the test specimen with the electrical contacts. The knife edges of the potential contacts are fixed at a distance of 2.00 centimeters. Electrical resistance measurements are then made by a commercially available potentiometer and a 0.001-ohm standard resistor.

For constant temperature control, measurements were made in a silicon fluid at 100° F (311 K). An immersion heater, placed horizontally along the bottom of the in-cell fixture tank, was controlled by a thermocouple mounted next to the test specimen and a temperature controller located on the out-of-cell instrument panel. An electric stirrer provided circulation of the oil around the test specimen and helped maintain a uniform temperature throughout the tank.

The test equipment was not available prior to the irradiation of the test specimens and therefore preirradiation measurements were not obtained. Thus, the change in electrical resistivity due to irradiation was calculated by using an average electrical resistivity value obtained from the set of unirradiated control specimens.

TEST RESULTS

Neutron Flux

The results of activation analyses of the flux monitor wires located along the irradiation capsule centerline are tabulated in table II and plotted, relative to the reactor core horizontal midplane, in figure 16. Three additional flux profiles along the perimeter of the irradiation capsule were planned. However, the omission of the flux monitor wires during loading of the irradiation capsule prevented their determination. The integrated flux values (fluence) seen by each test specimen is tabulated in table III. Since the specimens are located outward from the irradiation capsule centerline, each should be corrected for flux gradient and tungsten perturbation. A variation in the B position of -1.6×10^{19} fast neutrons per square centimeter and -8.0×10^{19} thermal neutrons per square centimeter is indicated by the analysis of electrical resistivity data discussed in the section Electrical Resistivity.

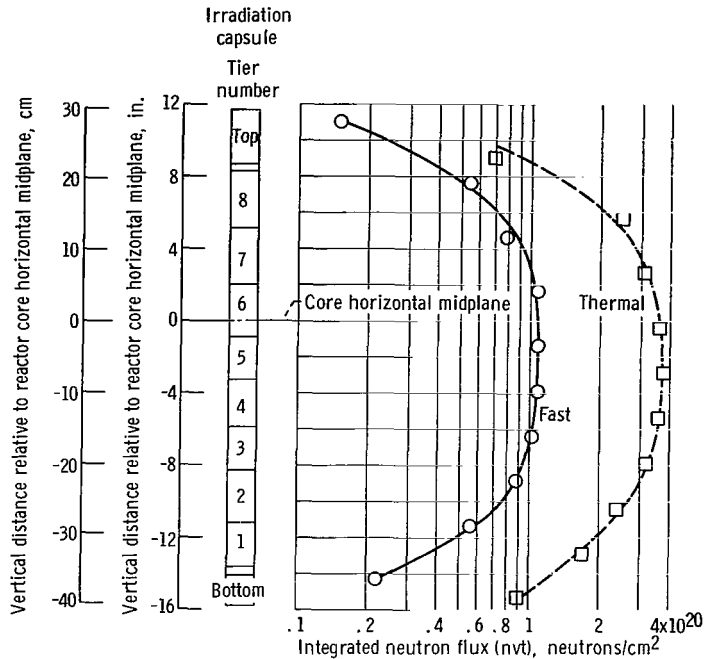


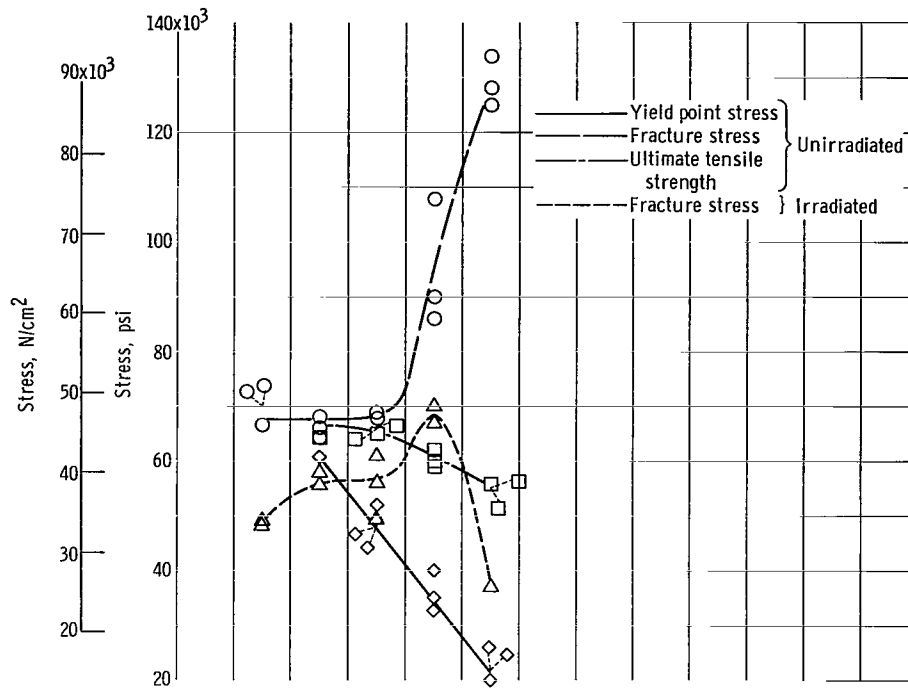
Figure 16. - Integrated fast and thermal neutron flux (nvt) profiles along center-line of irradiation capsule. Flux \approx nvt $\times 10^{-6}$.

Tensile Properties

The tensile test data in table IV are plotted as a function of test temperature in figure 17. Typical load-elongation curves for each test condition are shown in figure 18. The tensile data represent a single fracture within the gage length for all unirradiated test specimens and most of the irradiated test specimens. Double fractures did occur, however, during testing of three irradiated specimens. The irradiated test specimens were brittle; for example, five specimens were broken at room temperature during performance of nondestructive tests prior to tensile testing.

The yield stress data represent the point at which initial yielding was observed on the load-elongation curves. Yielding was generally a sharp transition followed by a Lüders strain region, although no drop in load occurred on yielding. For the unirradiated condition (fig. 18(a)), yielding occurred for tests conducted at 400^o F (477 K) and above. For the irradiated condition (fig. 18(b)), yielding did not occur up to and including 700^o F (644 K). The yield point stress for the unirradiated condition (fig. 17(a)) decreases linearly with increasing test temperature. Furthermore, the load-elongation curves (fig. 18(a)) show that the Lüders strain region also decreased with increasing test temperature and was only slightly evident in the 700^o (644 K) test data.

The ultimate tensile strength data represent the maximum load, after yielding, di-



(a) Tensile strength and stress.

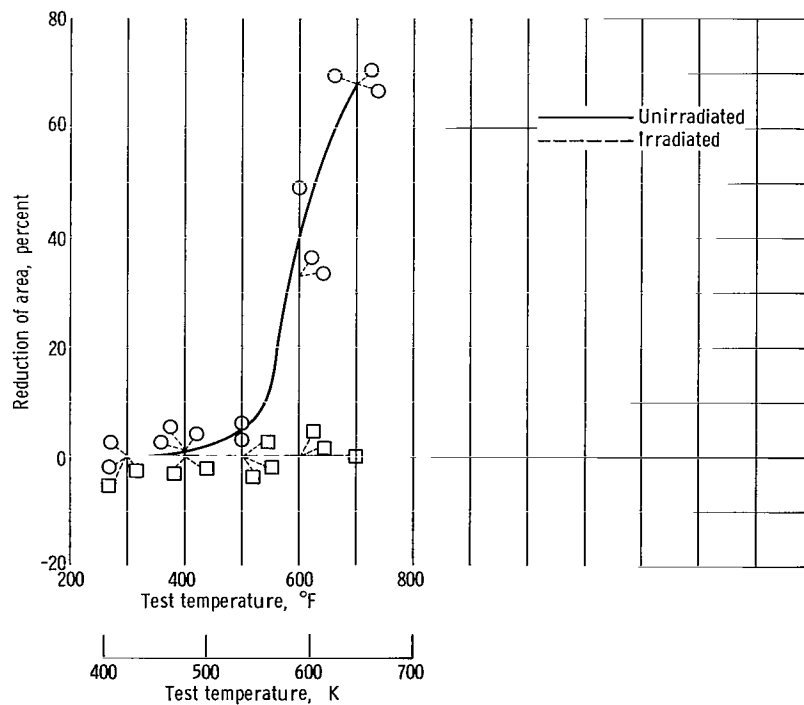


Figure 17. - Tensile properties as function of test temperature for unirradiated and irradiated tensile specimens.

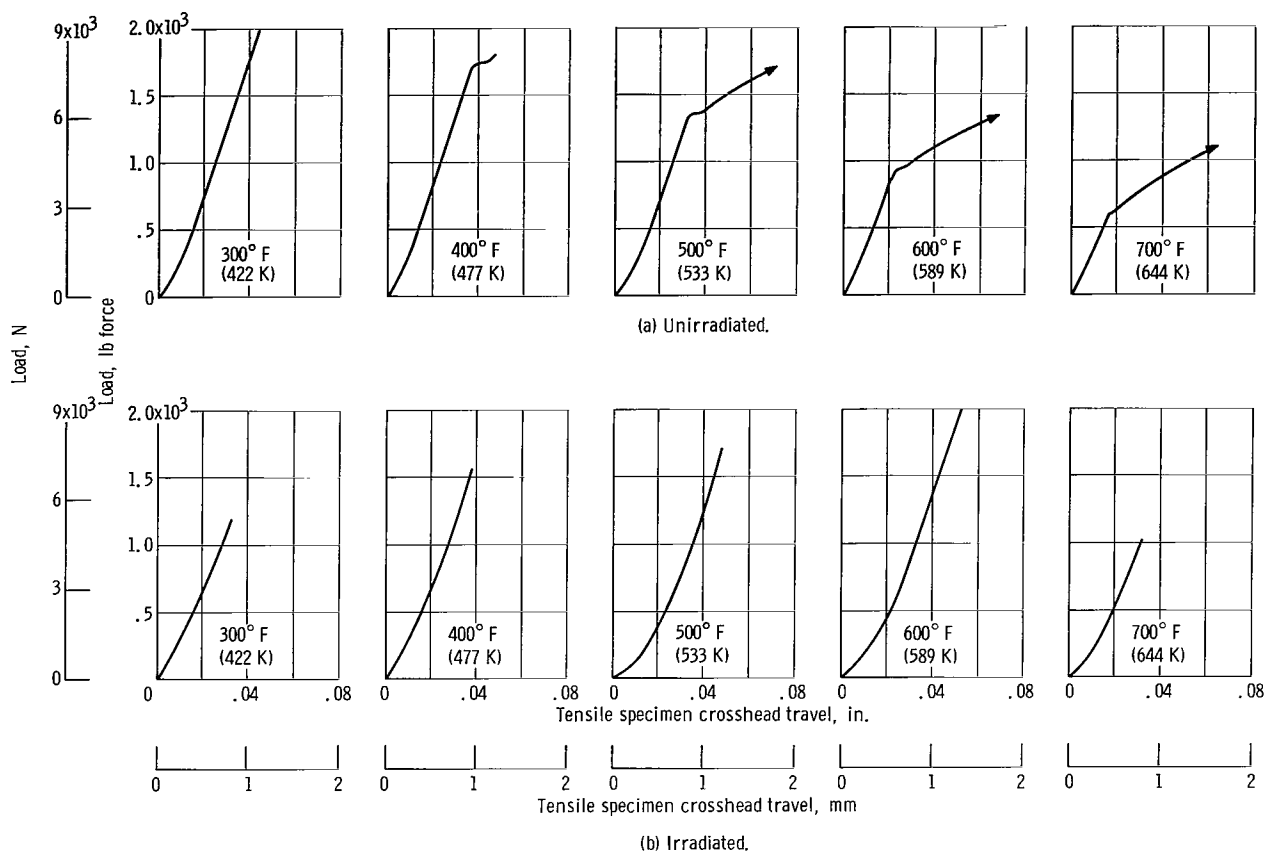


Figure 18. - Load as function of crosshead travel for unirradiated and irradiated tensile specimens.

vided by the original cross-sectional area of the test specimen. Since yielding did not occur for the irradiated condition, only unirradiated ultimate tensile strength data appear in figure 17(a). The unirradiated ultimate tensile strength, which is nearly equal to the unirradiated yield point stress at the 400° F (477 K) test temperature, decreases linearly, above about 500° F (533 K), with test temperature. The rate of decrease in ultimate tensile strength is less than the corresponding rate of decrease in yield point stress.

The reduction of area data (fig. 17(b)) show that, for the unirradiated condition, measurable plastic deformation occurs at about 400° F (477 K), and at test temperatures of 600° and 700° F (589 and 644 K), the unirradiated test material exhibits plastic deformation characteristic of ductile material. For the irradiated condition, the material failed without measurable plastic deformation at all test temperatures.

The fracture stress (fracture load divided by test specimen area following fracture) is reduced by the irradiation exposure (fig. 17(a)) for all test temperatures. The fracture stress of the irradiated material is, generally, greater than the yield point stress, but less than the ultimate tensile strength of the unirradiated material.

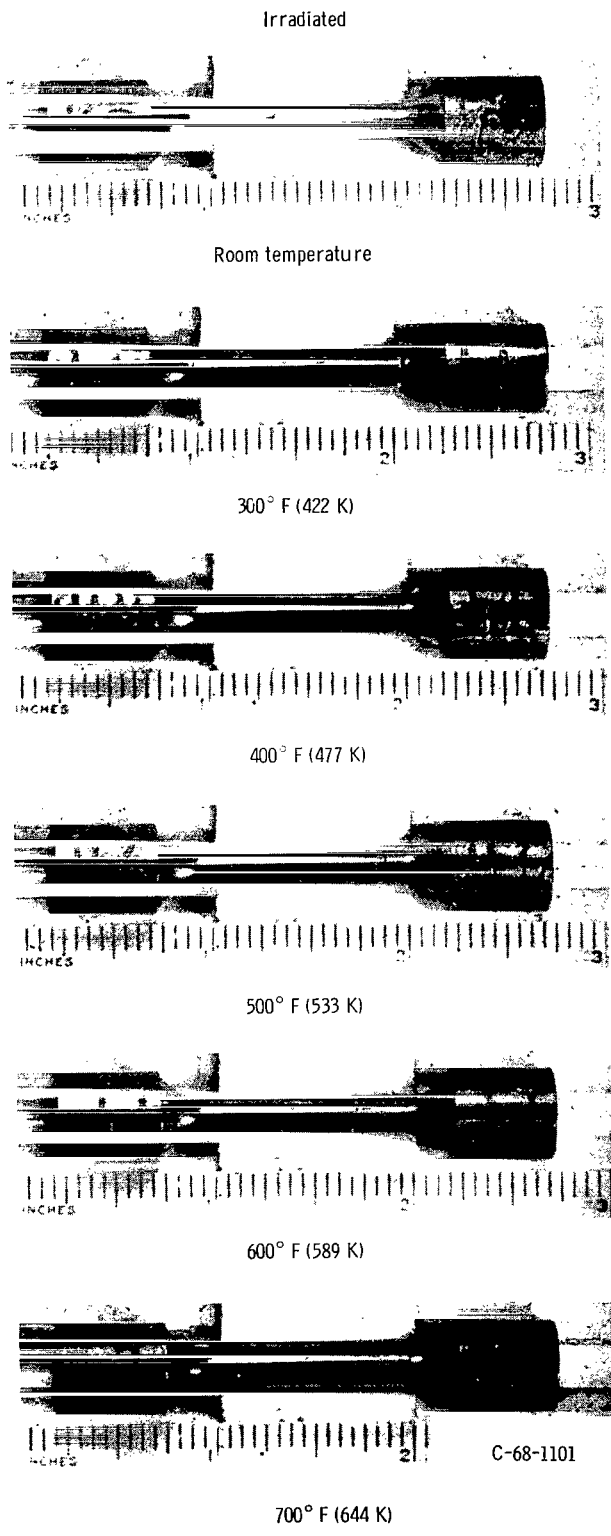
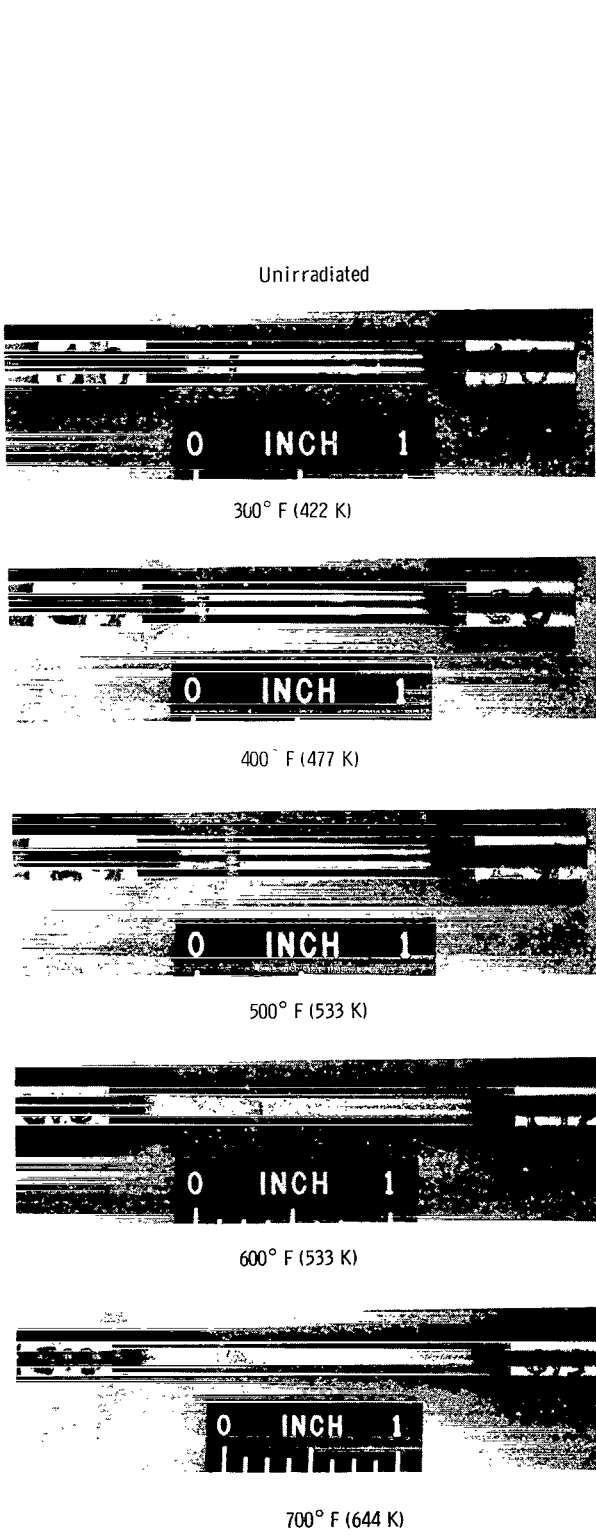


Figure 19. - Photomicrographs of unirradiated and irradiated tensile specimens.

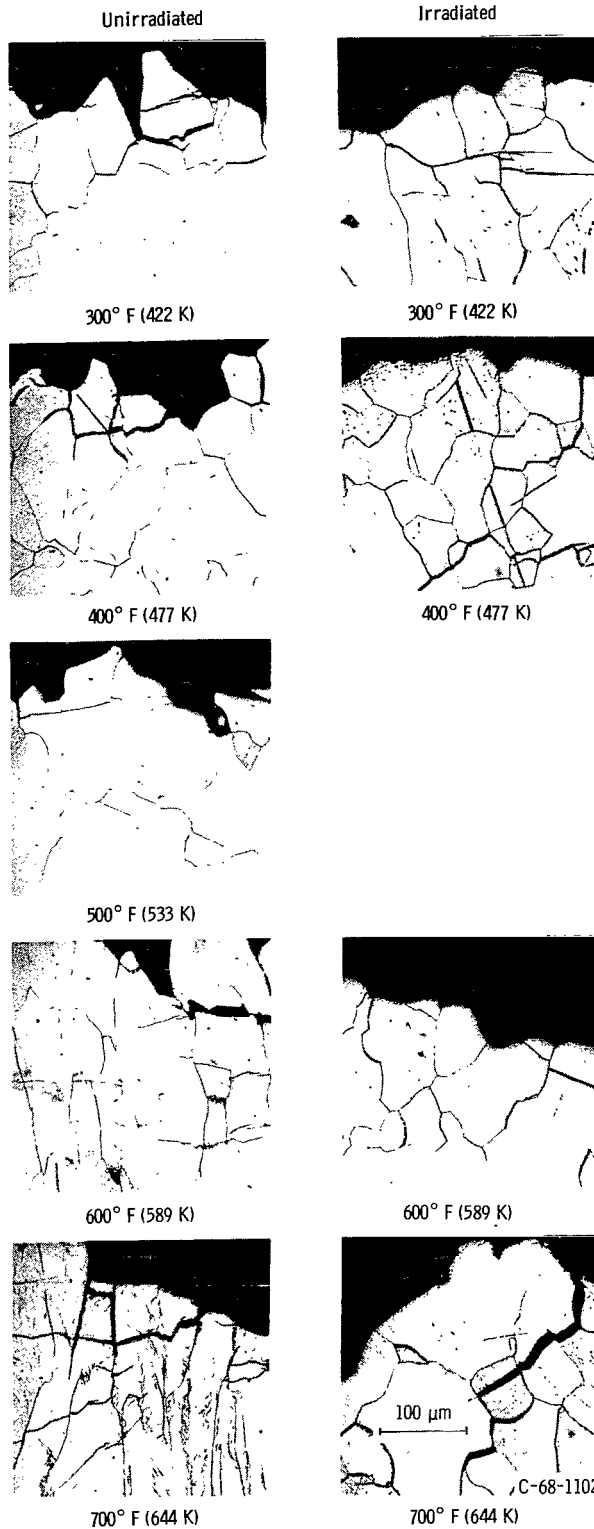


Figure 20. - Photomicrographs of unirradiated and irradiated tensile specimens. Etched with 75 grams of potassium ferricyanide ($K_3Fe(CN)_6$) and 20 grams of sodium hydroxide in 500 cubic centimeters of water. X125.

Figure 19 shows photomacrographs of unirradiated and irradiated tensile specimens fractured at the various test temperatures. For the unirradiated condition, the ductility at the higher test temperatures is evident, showing surface strain marks and necking at 700° F (644 K) prior to fracture. For the irradiated condition, all specimens show brittle fracture and no surface strain marks.

Figure 20 shows photomicrographs of unirradiated and irradiated tensile specimens fractured at the various test temperatures. For the unirradiated condition, the microstructure changes from an equiaxed grain structure at the lower test temperatures, to an elongated grain structure at the higher test temperatures. At the 500° F (533 K) test temperature, there is an indication of the elongated grain, but the predominant structure remains equiaxed. Similarly, the fracture mode in the unirradiated material changes at about 500° F (533 K), from brittle intergranular (low temperature type) to ductile transgranular (high temperature type). Transgranular microcracks are evident at all test temperatures; however, below 500° F (533 K), these microcracks are confined to individual grains immediately adjacent to the fracture. At 600° and 700° F (589 and 644 K), these transgranular microcracks traverse several grains, extending several grain diameters away from the fracture.

Photomicrographs (fig. 20) for the irradiated condition show an equiaxed grain structure and brittle intergranular fracture over the entire range of temperatures investigated. There is no apparent difference in the microstructures of the irradiated material tested at 400°, 600°, and 700° F (477, 589, and 644 K). At 300° F (422 K), the irradiated test material shows transgranular microcracks located several grain diameters away from the fracture. At all test temperatures, the microstructure of the irradiated material is similar to the 300° F (422 K) microstructure of the unirradiated material.

These tensile test results show that irradiation increases the yield point stress but decreases the grain boundary strength, as evidenced by the reduction in fracture stress, of polycrystalline tungsten. As a consequence of these effects, the temperature necessary for ductile behavior is increased by at least 300° F (167 K) from 400° F (477 K) to above 700° F (644 K).

Bend Properties

The results of bend tests are shown in table V and are plotted as a function of irradiation in figure 21. All specimens failed in a brittle manner with calculated bend angles less than 3°.

The data in table V indicate that electropolishing the test specimens prior to irradiation resulted in only a minor improvement in bend ductility. This is evidenced by a reduction in data scatter and a slight increase, about 7 percent, in the extreme fiber

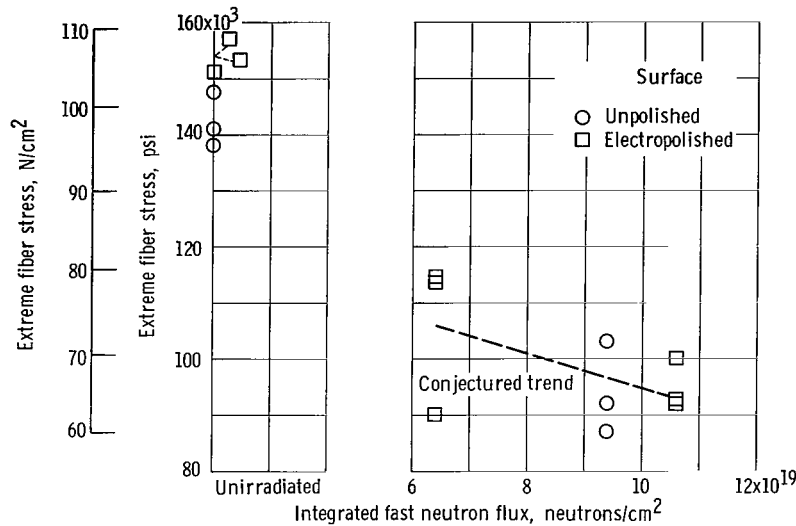


Figure 21. - Extreme fiber stress as function of integrated fast neutron flux.

stress of the electropolished specimens. The irradiated test data, although subject to considerable scatter, show that irradiation decreases the extreme fiber stress.

The data plotted in figure 21 show that the reduction in extreme fiber stress appears to be dependent on the integrated neutron flux. For neutron irradiations of 6.4×10^{19} neutrons per square centimeter the reduction in extreme fiber stress is about 30 percent, and for 1.06×10^{20} neutrons per square centimeter it is about 35 percent.

Photomicrographs of bend specimens are shown in figure 22. These photomicrographs show that all fractures were brittle intergranular with only minor differences due to exposure and/or test condition. For the unirradiated material, the photomicrographs show transgranular microcracks in electropolished material but none in the as-ground and annealed material. Transgranular microcracking is associated with more ductile material. For the irradiated material, transgranular microcracking is not apparent, and grain boundary separation is considerably enhanced. These test results show that the irradiation decreased the grain boundary strength and thus lowered the extreme fiber stress.

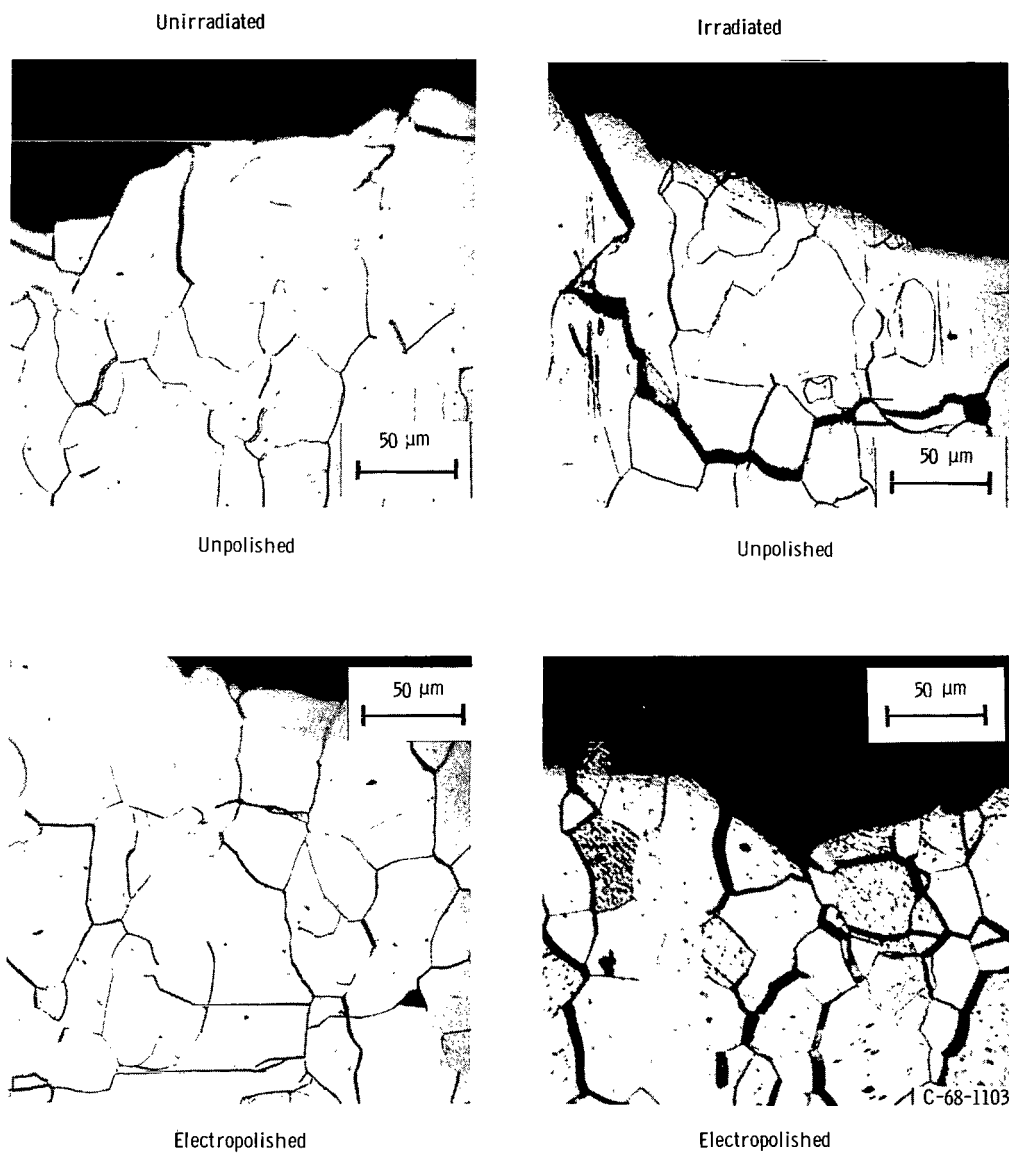
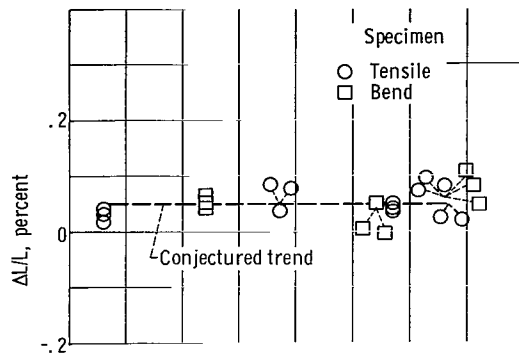
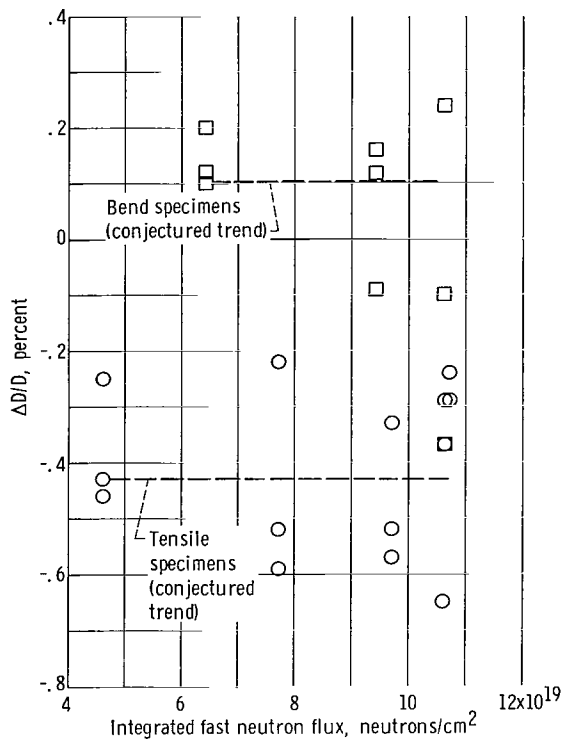


Figure 22. - Photomicrographs of unirradiated and irradiated bend specimens. Etched with 75 grams of potassium ferricyanide ($K_3Fe(CN)_6$) and 20 grams of sodium hydroxide in 500 cubic centimeters of water. X250.



(a) Length change.



(b) Diameter change.

Figure 23. - Dimensional changes as function of integrated fast neutron flux.

irradiation exposure are compiled in table VII.

The data from table VII are plotted as a function of centerline flux in figures 24 and 25 where it may be seen that the decrease in density, about 0.1 gram per cubic centimeter (or about 0.4 percent), is accompanied by volume expansion. The decrease in density (fig. 24) does not appear to be strongly influenced by differences in integrated neutron flux. Volume expansion (fig. 25(b)), however, does appear to depend on the integrated neutron flux. Up to about 5×10^{19} fast neutrons per square centimeter, the volume apparently increases to some limiting value and then decreases with additional ir-

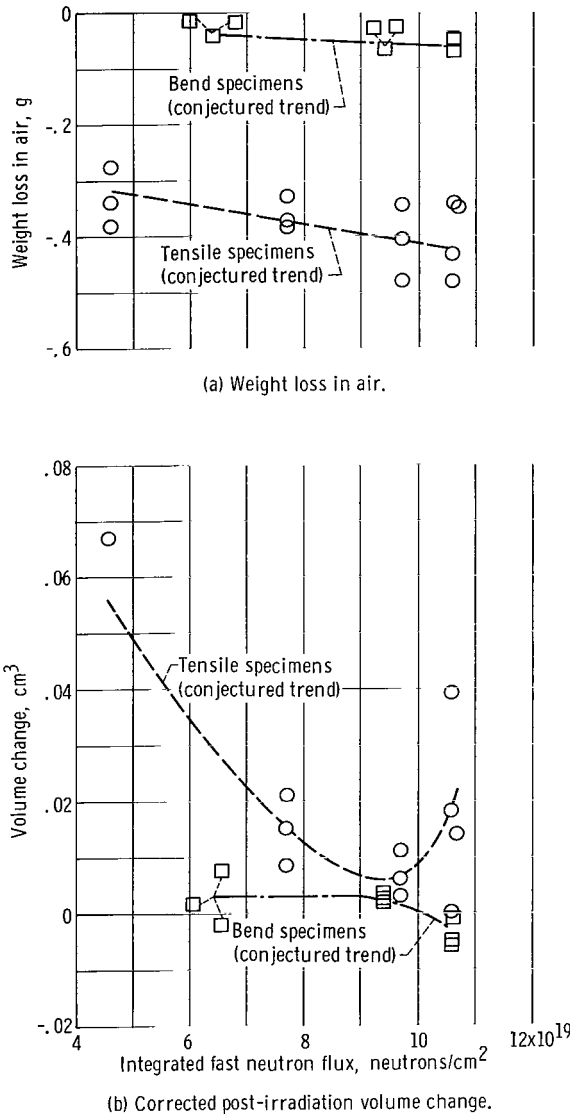


Figure 25. - Weight loss in air and corrected post-irradiation volume change as function of integrated fast neutron flux.

radiation. At about 1×10^{20} fast neutrons per square centimeter, the volume change is essentially zero, and for greater exposures, the trend is not readily apparent since tensile test specimens show volume expansion, but bend test specimens show further volume contraction.

The weight change in air following irradiation exposure (fig. 25(a)) appears to decrease linearly with increasing integrated neutron flux and also appears to be dependent on the surface area of the test specimen.

Electrical Resistivity

Electrical resistivity measurements, along with the change due to irradiation, are given in table VIII. In addition to measured values, a normalized value consists of dividing the measured electrical resistivity by its corresponding postexposure density (table VII) value. The variation of electrical resistivity with density for unirradiated

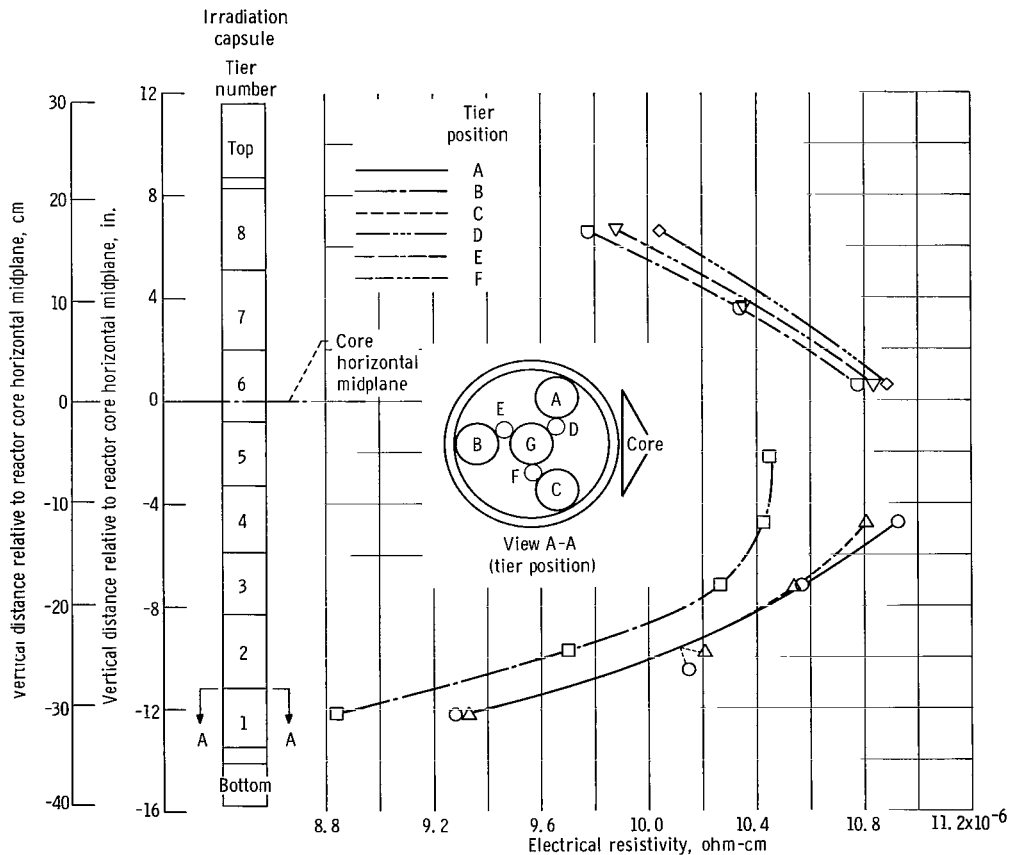
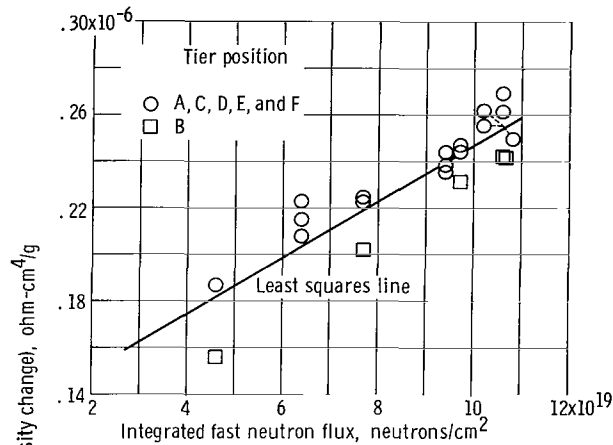


Figure 26. - Electrical resistivity as function of exposure location.

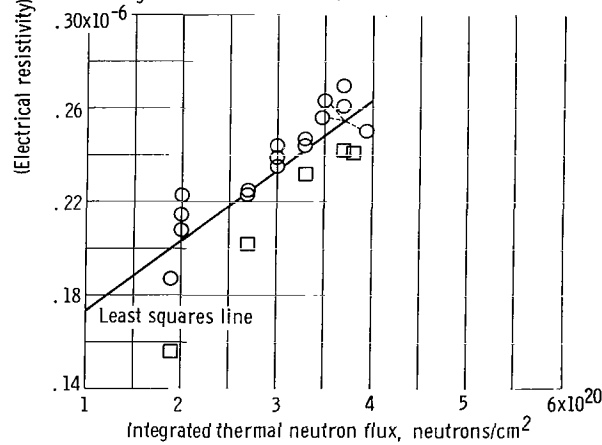
tungsten is discussed by Smithells (ref. 17).

Inspection of table VIII shows that the electrical resistivity of tensile test specimens irradiated in the B position of each capsule tier is significantly lower than that for tensile test specimens irradiated in the A and C positions. The irradiated electrical resistivity data from table VIII are plotted according to specimen position in figure 26. This plot shows that the effect of irradiation on electrical resistivity depends on both the distance above or below the horizontal midplane as well as the specimen position within a given tier. Furthermore, the shape of the family of curves (fig. 26) resembles the centerline flux profiles in figure 16.

In figure 27(a), the electrical resistivity data are replotted as a function of inte-



(a) (Electrical resistivity)/(Density change) as function of integrated fast neutron flux.



(b) (Electrical resistivity)/(Density change) as function of integrated thermal neutron flux.

Figure 27. - (Electrical resistivity)/(Density change) as function of integrated fast and thermal neutron flux.

grated fast neutron flux as determined from the centerline flux profile of figure 16. The response curve shown in figure 27(a) is a straight line, fit by the method of least squares, and indicates that the electrical resistivity increases linearly with increasing integrated fast neutron flux. Figure 27(b) shows essentially the same response when the data are plotted against the integrated thermal neutron flux.

Figure 27 also shows that, in all cases, the data for specimens located in position B of each capsule tier is low, as might be expected because of flux perturbations. Based on these data, it appears that the flux perturbation is greater for specimens located in position B and amounts to 1.6×10^{19} fast neutrons per square centimeter and 8.0×10^{19} thermal neutrons per square centimeter.

DISCUSSION OF TEST RESULTS

The ductile-to-brittle transition behavior of recrystallized tungsten, in the unirradiated condition, is markedly dependent on factors which influence localized stress concentrations, crack initiation, and crack propagation. The literature contains numerous detailed discussions of the dislocation mechanics (e. g., refs. 1, 8, and 18 to 22), and the effects of variables which influence crack initiation and propagation (e. g., see refs. 8 and 23 to 28).

Test results from the present investigation show that, for an irradiation of about 1×10^{20} fast neutrons per square centimeter, the ductile-to-brittle transition temperature is increased by at least 300° F (167 K). This increase in ductile-to-brittle transition temperature is accompanied by an increase in the temperature-dependent yield point stress and decreases in the tensile fracture and extreme fiber bending stresses. Furthermore, the irradiation effect appears to be the result of factors which decrease grain boundary strength (i. e., enhance intergranular fracture) and inhibit transgranular fracture.

Although the test program and test data obtained do not permit analyses of the basic mechanisms of the radiation-metal interactions, the effects associated with surface condition, impurities, and metallurgical defects warrant further discussion.

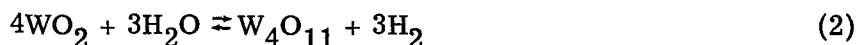
Surface Condition

Surface preparation can significantly influence the ductile-to-brittle transition behavior of tungsten (e. g., see refs. 9, 25, 29, and 30). For this reason, test specimen gage sections were electropolished prior to testing to eliminate possible surface contaminants and minimize surface roughness.

Diameter and weight measurements (tables VI and VII) showed that material had been lost from the specimen surfaces because of irradiation exposure and/or postirradiation storage. These changes were small, but exceeded the uncertainty of measurements and therefore appeared to be real. As a consequence of the surface material lost, the gage sections of the irradiated test specimens cannot be considered as having smooth electropolished surfaces.

Since the test specimens were immersed in water during irradiation exposure and postirradiation storage prior to testing, corrosion is one of the more probable explanations of the observed changes. Corrosion of tungsten by the water environment was not expected to occur and therefore deserves reevaluation, even though corrosion kinetics are beyond the scope of the present investigation.

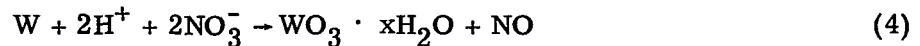
The corrosion of tungsten by water involves three equilibrium states indicated by the following equations:



At 200° F (366 K), in the absence of irradiation, these oxidation-reduction reactions do not proceed at a detectable rate (e. g., see refs. 6, 7, 17, and 31 to 34). If corrosion is the operating mechanism, the reaction rates for oxidation-reduction must be changed by the irradiation exposure. Experimental work by Smoluchowski and coworkers (refs. 35 and 36) with high-energy protons shows that the electrode potential of recrystallized tungsten becomes more anodic when irradiated. Similar changes in reactivity would probably occur with neutron irradiation, although there are no known experimental investigations to support this postulation.

The oxidation-reduction reactions (eqs. (1) to (3)) are accompanied by characteristic color transitions depending on the tungsten oxide (ref. 17): WO_2 is a dense, adherent oxide of chocolate-brown color, W_4O_{11} is a dense, adherent oxide whose color is violet, and WO_3 is a highly porous, volatile oxide of yellow color. Visual inspection of the test specimens following irradiation showed no adverse effects due to water exposure. The test specimen gage sections appeared smooth, retaining their original electropolished luster, and gave no evidence of color change which would indicate oxide formation. Therefore, the corrosion mechanism is not simply a change in reactivity, but rather requires some mechanism which oxidizes tungsten directly to the volatile WO_3 form and then removes this oxide. One possible reaction is nitric acid attack which readily con-

verts tungsten to the yellow oxide (ref. 37):



Water dissociation and nitrogen fixation are well-known problems associated with operating water-cooled nuclear power plants (e. g. , see refs. 38 and 39). Nitrogen fixation leads to the formation of nitric acid and the probable reaction noted in equation (4). The cooling water flowing during irradiation could easily remove the volatile WO_3 . During postirradiation storage, the rate of the suggested reaction is essentially zero, and hence the absence of characteristic oxide colors can be explained.

It therefore appears that the reduction in test specimen diameters and weights is primarily the result of an alteration of the exposure medium (water). As a consequence, a chemically etched surface condition is probably representative of the irradiated test specimens.

Stephens (ref. 29) investigated the effect of various surface conditions, including chemical etching, on the ductile-to-brittle transition temperature of unirradiated tungsten. His test results show that chemical etching increases the ductile-to-brittle transition temperature by 35° to 85° F (22 to 47 K). Embrittlement of the irradiated test material in the present program is therefore attributable, in part, to surface effects.

It is significant to note, however, that at 500° F (533 K) Stephens (ref. 29) reports measurable plastic deformation for sharply notched surface conditions of unirradiated tungsten. Since no measurable plastic deformation was observed for the irradiated test material up to 700° F (644 K), the greater portion of the increase in ductile-to-brittle transition temperature, at least 215° F (120 K), must be caused by mechanisms other than surface effects.

Impurities

The adverse effect of impurities on the ductile-to-brittle transition behavior of unirradiated tungsten is well known (e. g. , see refs. 1, 7, 8, 23, and 24). In general, impurities may influence the transition behavior in one of two ways. They can increase dislocation pile up, and as a consequence, brittle fracture at lower temperatures. The transition from ductile to brittle behavior therefore occurs at higher test temperatures. The second general adverse effect is associated with the low solubility limits of tungsten for impurities. Here impurities segregate to grain boundaries and lower the stress for crack initiation and propagation.

As noted previously, the tensile test data for the present investigation indicates that irradiation increases the yield point stress and decreases the grain boundary strength.

The test material used in the program was of commercial purity and contained small amounts of impurities, notably carbon (22 to 15 ppm), oxygen (11 ppm) and molybdenum (10 ppm). The 0.125-inch (3.2-mm) rod material also contained 18 ppm of sulfur while the 0.500-inch (12.7-mm) rod material contained 10 ppm of aluminum. In addition to impurities present in the unirradiated material, transmutation of about 1 percent of the tungsten to rhenium occurred as a result of neutron capture during irradiation.

Carbon. - Low levels of carbon impurity are known to affect the ductile-to-brittle transition behavior of polycrystalline tungsten. Stephens (ref. 40) reports that with increasing carbon impurity content between 8 and 60 ppm, the strength and ductile-to-brittle transition temperature increase correspondingly. Test data, the ductile-to-brittle transition temperature and the strength values, reported herein for material containing 22 ppm carbon fall intermediate to Stephens' materials containing 8 and 36 ppm carbon impurities.

Stephens (ref. 40) also shows that the fracture mode associated with carbon impurities is predominately transgranular. Photomicrographs of the unirradiated test material reported herein also show, particularly at the higher test temperatures, that fracture is predominately transgranular. For the irradiated material, the fracture is predominately intergranular. This intergranular fracture mode and the increase in fracture stress of the irradiated material suggests that transgranular crack initiation due to carbon impurities has been impeded by defects introduced by irradiation. Additional support for this effect may be seen in the photomicrographs. For the unirradiated condition, large inclusions, precipitates, and second phases at the grain boundaries may be observed. The photomicrographs of the irradiated material, however, show precipitates which appear to be held within the grain.

Oxygen. - Recent experimental data by Stephens (refs. 40 and 41) show that oxygen is a significant factor in ductile-to-brittle transition behavior. With increasing oxygen content between 4 and 50 ppm, the ductile-to-brittle transition temperature of polycrystalline tungsten increased proportionally. This increase in ductile-to-brittle transition temperature was accompanied by corresponding decreases in yield strength. The fracture mode was predominately intergranular over the temperature range up to 1000^o F (811 K).

The test material for the program reported herein contained 11 ppm oxygen impurity, and test results for unirradiated material are in agreement with Stephens' data. Although the test results for the irradiated material show a reduction in grain boundary strength, the low level of oxygen impurity and the increase in yield strength do not favor oxygen impurities as contributing significantly to the fracture mechanism.

Miscellaneous. - Of the other impurities present in the test material, aluminum may be effective in influencing ductile-to-brittle transition behavior since 30 ppm of aluminum impurity is known to influence the recrystallization behavior of tungsten (ref. 8).

Hydrogen and nitrogen may also influence the ductile-to-brittle transition behavior (ref. 23), but their contents in the material were not determined. The absence of data precludes discussion of the effects of these impurities, although by analogy, the effect of aluminum would probably be similar to carbon, while hydrogen and nitrogen would be similar to oxygen.

Rhenium. - In addition to impurities present in the unirradiated material, transmutation of tungsten to rhenium occurs as a result of neutron capture during the irradiation. For the irradiation employed herein, about 1 percent of the tungsten would undergo transmutation to rhenium. Moteff and Smith (ref. 42) performed annealing experiments on similar test material which had been irradiated under conditions similar to those reported herein. The results of these annealing experiments show that the electrical resistivity of irradiated material, following high-temperature anneals (2170 K), is greater than the unirradiated material and corresponds to the electrical resistivity of a tungsten - 1-percent-rhenium alloy.

The measured value of electrical resistivity for irradiated specimens (table VIII), is approximately 10 microhm-centimeters, which corresponds to that of tungsten - 3 percent rhenium (ref. 5). Since calculations by the authors and annealing experiments by Moteff and Smith indicate that transmutations correspond to only tungsten - 1 percent rhenium, the additional electrical resistivity increase is probably the result of metallurgical defects other than impurities.

It is interesting to note that density measurements (table VII) on bend test specimens irradiated in tier 6 of the irradiation capsule show an increase in density, while all other measurements show decreases in density. These specimens were subjected to the highest level of neutron flux, and calculations are in agreement with the density of tungsten - 1 percent rhenium. The reason for this anomalous behavior is not apparent from experimental results.

The significance of transmutation to the present discussion lies in the effects rhenium impurities have on the strength and ductile-to-brittle transition behavior of tungsten. Alloying of unirradiated tungsten with rhenium has increased the strength and lowered the ductile-to-brittle transition temperature for rhenium additions up to about 28 percent, the solubility limit (refs. 23 and 43). When subjected to irradiation, the material does increase in strength, but the ductile-to-brittle transition temperature also increased, which is contrary to the expected effect for alloying unirradiated material. The beneficial effect of rhenium in decreasing the ductile-to-brittle transition temperature may well be masked by other more detrimental effects leading to the decrease in grain boundary strength.

In view of the preceding discussion, the impurities present in the test material and that introduced by transmutation appear to contribute to the strength increase observed

in the irradiated material but do not explain the loss of grain boundary strength and the increase in ductile-to-brittle transition temperature.

Metallurgical Defects

The tungsten used in the present test program was prepared by powder metallurgy techniques. The metallurgical state therefore contains grain boundary voids, attributable to the sintering process (e. g. , see refs. 44 to 46). Electron microscope (refs. 47 and 48) and field ion microscope (refs. 49 and 50) studies of unirradiated tungsten show that voids ranging in size from a few angstroms to several hundred angstroms in diameter are also distributed within the grain as well as along grain boundaries.

Subjecting unirradiated material to elevated temperatures produces void coalescence and diffusion with reaction rates being dependent on many factors including fabrication history, time, temperature, and stress gradients. McCoy and Stiegler (refs. 51 and 52) studied the nucleation and growth of voids in unirradiated tungsten following creep rupture tests at elevated temperatures (1923 and 2475 K). Their results for material which had been fabricated by chemical vapor deposition show a network of large voids distributed throughout the grains and along grain boundaries. Lesser effects were observed for sintered material. These researchers attributed the growth of voids to be caused in part by stress-induced diffusion of vacancies into the voids.

During irradiation, diffusion-controlled reactions may be altered (ref. 53) resulting in coalescence of voids and/or other defects and diffusion of these defects to the grain boundaries. Reaction rates are again dependent on many factors including time, temperature, and stress gradients. The coalescence and diffusion of defects to the grain boundaries could also account, in part, for the observed grain boundary weakening.

Photomicrographs of the test material used herein do not show the presence of voids. However, the preirradiation density, about 19.2 grams per cubic centimeter, represents a void volume of about 0.5 percent, based on a theoretical density of 19.3 grams per cubic centimeter. Minor variations are also evident between individual test specimens. Following irradiation, the density decreased by about 0.4 percent, and analysis of the test data indicates that the decrease is the result of volume expansion.

The irradiated tensile data at 500^o F (533 K) exhibit scatter which may well be diffusion dependent. These tests employed a soaking time at test temperature of only 10 minutes. Several investigators (e. g. , refs. 8, 18, 42, and 54 to 56) have pointed out that structural defects are mobile at 500^o F (533 K) and therefore different results may be observed for longer soaking times at test temperature.

Void growth could account for the observed effects; however, the void volume size is too small to be detected by the optical microscope studies employed herein, and con-

clusive evidence is not apparent.

Defects other than voids are also present in crystalline materials, and irradiation introduces additional defects. Point defects, dislocation loops, and various types of defect clusters, introduced by irradiation have been cited as the mechanisms responsible for property changes (e. g., see refs. 57 to 61). When confined within the grains, these defects can promote lattice expansion (hence volume expansion), as well as influence dislocation pile up, which directly or indirectly can cause the strength of the metal to increase. Lattice expansion and dislocation pile up would also change the state of stress along grain boundaries and thereby contribute to the reduction in grain boundary strength.

The increase in electrical resistivity of the irradiated material (fig. 27) was previously discussed with regard to impurities. Here it was noted that, although some of the increase could be accounted for by transmutation of tungsten to rhenium, the greater percentage of the increase must be the result of metallurgical defects other than impurities. Void growth might be expected to account for an additional amount of the increase, but data reported by Smithells (ref. 17) shows essentially no change in electrical resistivity for unirradiated material of 18.45 to 19.23 grams per cubic centimeter density. It therefore appears that various solid-state defects are major contributors to the increase in electrical resistivity following irradiation. Other investigators (e. g., see refs. 54, 55, and 62 to 64) have observed similar increases in electrical resistivity of tungsten following irradiation and have drawn similar conclusions.

The results of irradiation studies reported by Gray and Cummings (ref. 65) on polycrystalline molybdenum are particularly noteworthy since tungsten and molybdenum exhibit similar characteristics. The crystalline structures and lattice parameters of these two metals are also nearly identical. Test results reported by Gray and Cummings show that for irradiation exposures up to about 5×10^{19} fast neutrons per square centimeter at about 310 K, the lattice parameter of molybdenum increases with irradiation exposure. The increase in lattice parameter reaches a maximum of about 0.05 percent at about 5×10^{19} fast neutrons per square centimeter and then decreases with further irradiation. For an irradiation exposure of 1.1×10^{20} fast neutrons per square centimeter, there was essentially no change in the lattice parameter, and for 1.2×10^{20} fast neutrons per square centimeter, a decrease of about 0.005 percent occurred. Corresponding data show the X-ray line width to increase continuously with irradiation to 1.2×10^{20} fast neutrons per square centimeter. These effects are interpreted to be caused by the influence of point defects up to about 5×10^{19} fast neutrons per square centimeter and then the influence of interstitial cluster growth for exposures greater than 5×10^{19} fast neutrons per square centimeter.

The test data reported herein exhibit characteristics similar to those of the molybdenum studied by Gray and Cummings. The expansion in dimensions and volume are in agreement with lattice parameter increases of about 0.05 percent. At about 5×10^{19} fast

neutrons per square centimeter, the increase in volume due to irradiation appears to be a maximum. For irradiation exposures greater than about 5×10^{19} fast neutrons per square centimeter, the change in volume decreases and becomes zero at about 1.1×10^{20} fast neutrons per square centimeter. Although this comparison is qualitative, it suggests that defect clusters are primarily responsible for producing the observed property changes.

In view of the preceding discussions, it appears that polycrystalline tungsten subjected to reactor irradiation of about 10^{20} fast neutrons per square centimeter is strengthened by transmutation of tungsten to rhenium and by the introduction of point defects and/or defect clusters. These defects promote lattice expansion which produces stress concentrations along grain boundaries and contributes to a reduction in grain boundary strength. Void growth may also be influential in contributing to these effects; however, photomicrographs and electrical resistivity data indicate that void growth is not apparent and probably would account for only a small percentage of overall effect.

SUMMARY OF RESULTS AND CONCLUSIONS

The effect of reactor irradiation on embrittlement of polycrystalline tungsten has been investigated by comparing ductile-to-brittle transition behavior of unirradiated and irradiated material. Tensile tests conducted in the range 300° to 700° F (422 to 644 K) were used to determine ductile-to-brittle transition behavior. Bend tests were also conducted at room temperature with both unirradiated and irradiated material to provide additional data for investigating irradiation embrittlement.

Tensile and bend test results show that recrystallized tungsten irradiated with 1×10^{20} fast neutrons per square centimeter (neutron energy greater than 1 MeV) is severely embrittled. The ductile-to-brittle transition temperature for the irradiated material increased by at least 300° F (167 K) and was accompanied by an increase in the temperature-dependent yield point stress and decreases in the tensile fracture and extreme fiber bending stresses. The embrittlement appears to be the result of factors which decrease grain boundary strength and inhibit transgranular fracture.

Additional radiation effects data were obtained for changes in specimen dimensions, density, and electrical resistivity. The changes in specimen dimensions following irradiation were small but were greater than the uncertainty of measurement. Test specimen lengths increased while diameters decreased. The decrease in diameter is believed to be the result of radiation-induced oxidation which probably masked the real effect of irradiation on the material.

Test specimen densities decreased (of the order of 0.4 percent) as a result of irradiation exposure, although one set of test specimens showed the density to increase.

When corrected for the loss of material due to probable radiation-induced corrosion, the volume of each irradiated test specimen was greater than its corresponding unirradiated volume, with the exception of the one set of specimens which showed an increase in density. The volume of these specimens decreased as a result of the irradiation exposure.

Test specimen electrical resistivity increased linearly with irradiation exposure. This increase was 87 percent at the highest level of irradiation.

The results from specimen dimensions, density, and electrical resistivity were used in an analysis to identify the probable mechanism responsible for the embrittlement observed in the tensile and bend tests. This analysis shows that the embrittling mechanism is not a simple, unique defect, but rather a number of defects whose influences are synergistic and depend on diffusion-controlled reactions. The principal conclusions drawn from this analysis are as follows:

1. The test specimen surfaces were roughened from corrosion during irradiation. This effect is believed to be caused by an irradiation-induced alteration of the exposure medium (water).

2. As a result of the surface roughening, the change in ductile-to-brittle transition temperature of irradiated material should be reduced by about 85° F (47 K). Thus, an adjusted increase in ductile-to-brittle transition temperature of irradiated material would be at least 215° F (120 K) rather than the 300° F (167 K) previously noted.

3. Transmutations of tungsten to rhenium occurred as a result of irradiation. The irradiated material is believed to represent a tungsten - 1-percent-rhenium alloy rather than unalloyed tungsten.

4. As a result of rhenium additions to tungsten, the strength of the material should increase, as was observed, but the ductile-to-brittle transition should decrease, rather than increase as the test data show.

5. The test material contained about 0.5 percent void volume prior to irradiation. During irradiation, voids probably grow, but test data do not provide conclusive evidence as to the size, distribution, and growth kinetics of these voids. The contribution of void growth to the embrittlement observed is believed to be of only minor significance.

6. The effect of point defects, dislocation loops, and various defect clusters introduced by irradiation appear to be explained best by the yield point stress increase and the loss of grain boundary strength resulting in decreased tensile fracture and extreme fiber bending stresses. These defects can also account for the increase in ductile-to-brittle transition temperature.

It may be concluded, therefore, that irradiation of unalloyed, polycrystalline tungsten with 10^{20} fast and 10^{21} thermal neutrons per square centimeter produces a very

brittle tungsten - 1-percent-rhenium alloy. The strength of this alloy is greater than the starting material, but because of the presence of irradiation-induced point defects, dislocation loops, and various defect clusters, the grain boundary strength of the alloy is lower than the starting material.

Lewis Research Center,
National Aeronautics and Space Administration,
Cleveland, Ohio, March 22, 1968,
122-29-05-01-22.

APPENDIX A

ACTIVATION EQUATION FOR CALCULATING THERMAL NEUTRON FLUX

The thermal neutron flux was calculated from the cobalt 59 (neutron, gamma) cobalt 60 ($\text{Co}^{59} (n, \gamma) \text{Co}^{60}$) reaction by using the activation equation modified for burnup of Co^{59} and Co^{60} (ref. 66). This equation is

$$A_{60}(T, t) = \frac{N_0 \sigma_{59} \lambda_{60} \phi_{th}}{\phi_{th} \sigma_{60} + \lambda_{60} - \phi_{th} \sigma_{59}} \left\{ \exp(-\phi_{th} \sigma_{59} T) - \exp[-(\phi_{th} \sigma_{60} + \lambda_{60}) T] \right\} \exp(-\lambda_{60} t)$$

where

$A_{60}(T, t)$	Co^{60} activity, dis/sec/flux monitor wire
N_0	number of Co^{59} atoms in flux monitor wire at time zero
σ_{59}	thermal neutrons cross section for Co^{59} , 37 b
σ_{60}	thermal neutron cross section for Co^{60} , 6 b
λ_{60}	decay constant of Co^{60} , 4.18×10^{-9} /sec
ϕ_{th}	thermal neutron flux, neutrons/(cm^2)(sec)
T	irradiation time, sec
t	elapsed time between discharge from reactor field and counting, sec

APPENDIX B

ACTIVATION EQUATION FOR CALCULATING FAST NEUTRON FLUX

The fast neutron flux greater than 1 MeV was calculated from the nickel 58 (neutron, proton) cobalt 58 ($\text{Ni}^{58}(n, p) \text{Co}^{58}$) reaction by assuming a fission-neutron spectral shape, with modification for nuclear isomerism and burnup of Co^{58m} and Co^{58} (refs. 66 and 67). The equation used was as follows:

$$\begin{aligned}
 A_{58}(T, t) = & \frac{\lambda_{58} \lambda_{58m} N_{58m}}{\lambda_{58} - \lambda_{58m}} \left[1 - \exp(-\lambda_{58m}^* T) \right] \left[\exp(-\lambda_{58m} t) - \exp(-\lambda_{58} t) \right] \\
 & + \frac{\lambda_{58} \lambda_{58m} N_{58m}}{\lambda_{58}^* - \lambda_{58m}^*} \left[\exp(-\lambda_{58}^* T) - \exp(-\lambda_{58m}^* T) \right] \exp(-\lambda_{58} t) \\
 & + \lambda_{58} N_{58} \left[1 - \exp(-\lambda_{58}^* T) \right] \exp(-\lambda_{58} t)
 \end{aligned}$$

where

$A_{58}(T, t)$ Co^{58} activity, dis/sec/flux monitor wire

$$N_{58m} = \frac{(\sigma_{58m})_f N_o \phi_f}{0.693 \lambda_{58m}^*}$$

$$N_{58} = \frac{(\sigma_{58})_f N_o \phi_f}{0.693 \lambda_{58}^*} + \frac{\lambda_{58m} (\sigma_{58m})_f N_o \phi_f}{0.693 \lambda_{58}^* \lambda_{58m}^*}$$

$$\lambda_{58m}^* = \lambda_{58m} + (\sigma_{58m})_{th} \phi_{th}$$

$$\lambda_{58}^* = \lambda_{58} + (\sigma_{58})_{th} \phi_{th}$$

where

N_o number of Ni^{58} atoms in flux monitor wire at time zero

$(\sigma_{58m})_f$ fission neutron cross section for production of Co^{58m} , 28 mb

$(\sigma_{58})_f$ fission neutron cross section for production of Co^{58} , 63 mb

$(\sigma_{58m})_{th}$	thermal neutron cross section of Co^{58m} , 1.7×10^5 b
$(\sigma_{58})_{th}$	thermal neutron cross section of Co^{58} , 1.65×10^3 b
λ_{58m}	decay constant of Co^{58} , 2.14×10^5 /sec
λ_{58}	decay constant of Co^{58} , 1.13×10^{-7} /sec
ϕ_f	fast neutron flux, neutrons/(cm ²)(sec)
ϕ_{th}	thermal neutron flux, neutrons/(cm ²)(sec)
T	irradiation time, sec
t	elapsed time between discharge from reactor field and counting, sec

REFERENCES

1. Bechtold, J. H. ; Wessel, E. T. ; and France, L. L. : Mechanical Behavior of the Refractory Metals. Refractory Metals and Alloys. Vol. 11 of Metallurgical Society Conferences. M. Semchyshen and J. J. Harwood, eds. , Interscience Publishers, Inc. , 1961, pp. 25-81.
2. Makin, M. J. ; and Gillies, E. : The Effect of Neutron Irradiation on the Mechanical Properties of Molybdenum and Tungsten. J. Inst. Metals, vol. 86, 1957-1958, pp. 108-112.
3. Sutton, C. R. ; and Leeser, D. O. : Radiation Effects on Structural Materials. Chem. Eng. Prog. Symp. Ser. , vol. 50, no. 12, 1954, pp. 208-221.
4. Barth, V. D. : Physical and Mechanical Properties of Tungsten and Tungsten-Base Alloys. DMIC Rep. 127, Battelle Memorial Inst. , Mar. 15, 1960.
5. Schmidt, F. A. ; and Ogden, H. R. : The Engineering Properties of Tungsten and Tungsten Alloys. DMIC Rep. 191, Battelle Memorial Inst. , Sept. 27, 1963. (Available from DDC as AD-425547.)
6. Syre, R. : Handbook on the Properties of Niobium, Molybdenum, Tantalum, Tungsten, and Some of Their Alloys. AGARDograph 94, North Atlantic Treaty Organization, Advisory Group for Aerospace Research and Development, Paris, France, 1965.
7. Tietz, T. E. ; and Wilson, J. W. : Behavior and Properties of Refractory Metals. Stanford University Press, 1965.
8. Atkinson, R. H. ; Keith, G. H. ; and Koo, R. C. : Tungsten and Tungsten-Base Alloys. Refractory Metals and Alloys. Vol. 11 of Metallurgical Society Conferences. M. Semchyshen and J. J. Harwood, eds. , Interscience Publishers, Inc. , 1961, pp. 319-355.
9. Stephens, Joseph R. : An Exploratory Investigation of Some Factors Influencing the Room-Temperature Ductility of Tungsten. NASA TN D-304, 1960.
10. Donoughe, Patrick L. ; and Younger, Charles L. : Capsules for Surveillance of Some Plum Brook Reactor Structural Materials. Symposium on Problems in Irradiation Capsule Experiments, Germantown, Maryland, Oct. 8-10, 1963. William L. R. Rice, ed. AEC Rep. TID-7697, Mar. 1964, pp. 1.1.1-1.1.22.
11. Bagwell, David: TØSS - An IBM-7090 Code for Computing Transient or Steady State Temperature Distributions. Rep. K-1494, Oak Ridge Gaseous Diffusion Plant, Dec. 1, 1961.

12. Oldrieve, Robert E. : NASA Plum Brook Reactor Hot Laboratory Facility. Proceedings of the Ninth Conference on Hot Laboratories and Equipment. Paul R. Fields, ed., American Nuclear Society, Inc., 1961, pp. 44-55.
13. Jones, M. H. ; and Brown, W. F., Jr. : An Axial Loading Creep Machine. ASTM Bull. No. 211, Jan. 1956, pp. 53-60.
14. Stratton, K. : Density Measurement Problems in Hot Cells. Sixth Hot Laboratories and Equipment Conference, Mar. 19-21, 1958, Chicago. Frank Ring, Jr., Comp. AEC Rep. TID-7556, Apr. 1959, pp. 81-95.
15. Boyd, C. L. : A Technique for Measurement of Electrical Resistivity of Radioactive Metals. Symposium on Radiation Effects on Materials. Vol. 2. Spec. Tech. Pub. No. 220, ASTM, 1958, pp. 49-52.
16. Stang, L. G., Jr., Comp. : Electrical-Resistivity Measuring Apparatus. Hot Laboratory Equipment. Second ed. USAEC, 1958, pp. 278-279.
17. Smithells, Colin J. : Tungsten, Its Metallurgy, Properties, and Applications. Chemical Publishing Co., Inc., 1953.
18. Wronski, A. S. ; Sargent, G. A. ; and Johnson, A. A. : Irradiation Hardening and Embrittlement in Body-Centered Cubic Transition Metals. Symposium on Flow and Fracture of Metals and Alloys in Nuclear Environments. Spec. Tech. Pub. No. 380, ASTM, 1965, pp. 69-85.
19. Johnson, A. A. : Deformation, Fracture, and Radiation Damage, in Body-Centered Cubic Transition Metals. J. Less-Common Metals, vol. 2, 1960, pp. 241-252.
20. Owen, W. S. ; and Hull, D. : The Fracture Transitions in Refractory Metals. Refractory Metals and Alloys, II. Vol. 17 of Metallurgical Society Conferences. M. Semchyshen and I. Perlmutter, eds., Interscience Publishers, Inc., 1963, pp. 1-21.
21. Conrad, H. : The Cryogenic Properties of Metals. High Strength Materials. Victor F. Zackay, ed., John Wiley & Sons, Inc., 1965, pp. 436-509.
22. Amelinckx, S. ; and Dekeyser, W. : The Structure and Properties of Grain Boundaries. Solid State Physics; Advances in Research and Applications. Vol. 8. Frederick Seitz and David Turnbull, eds., Academic Press, Inc., 1959, pp. 325-499.
23. Hahn, G. T. ; Gilbert, A. ; and Jaffee, R. I. : The Effect of Solutes on the Ductile-to-Brittle Transition in Refractory Metals. Refractory Metals and Alloys, II. Vol. 17 of Metallurgical Society Conferences. M. Semchyshen and I. Perlmutter, eds., Interscience Publishers, Inc., 1963, pp. 23-63.

24. Armstrong, R. W.; Bechtold, J. H.; and Begley, R. T.: Mechanisms of Alloy Strengthening in Refractory Metals. Refractory Metals and Alloys, II. Vol. 17 of Metallurgical Society Conferences. M. Semchyshen and I. Perlmutter, eds., Interscience Publishers, Inc., 1963, pp. 159-190.
25. Seigle, L. L.; and Dickinson, C. D.: Effect of Mechanical and Structural Variables on the Ductile-Brittle Transition in Refractory Metals. Refractory Metals and Alloys, II. Vol. 17 of Metallurgical Society Conferences. M. Semchyshen and I. Perlmutter, eds., Interscience Publishers, Inc., 1963, pp. 65-116.
26. Rapperport, E. J.; and Hartley, C. S.: A Review of Diffusion in Refractory Metal Systems. Refractory Metals and Alloys II. Vol. 17 of Metallurgical Society Conferences. M. Semchyshen and I. Perlmutter, eds., Interscience Publishers, Inc., 1963, pp. 191-221.
27. Weissman, S.; Lement, B. S.; and Cohen, Morris: Substructure in Refractory Metals. Refractory Metals and Alloys, II. Vol. 17 of Metallurgical Society Conferences. M. Semchyshen and I. Perlmutter, eds., Interscience Publishers, Inc., 1963, pp. 117-158.
28. Reid, C. N.: A Review of Mechanical Twinning in Body-Centered Cubic Metals and Its Relation to Brittle Fracture. J. Less-Common Metals, vol. 9, 1965, pp. 105-122.
29. Stephens, Joseph R.: Effect of Surface Condition on Ductile-to-Brittle Transition Temperature of Tungsten. NASA TN D-676, 1961.
30. Stephens, J. R.: Effect of Surface Condition on the Ductility of Tungsten. High Temperature Materials, II. Vol. 18 of Metallurgical Society Conferences. G. Mervin Ault, W. F. Barclay, and H. P. Munger, eds., Interscience Publishers, Inc., 1963, pp. 125-137.
31. Kubaschewski, O.; and Hopkins, B. E.: Oxidation Mechanisms of Niobium, Tantalum, Molybdenum and Tungsten. J. Less-Common Metals, vol. 2, 1960, pp. 172-180.
32. Semmel, J. W., Jr.: Oxidation Behavior of Refractory Metals and Alloys. Refractory Metals and Alloys. Vol. 11 of Metallurgical Society Conferences. M. Semchyshen and J. J. Harwood, eds., Interscience Publishers, Inc., 1961, pp. 119-168.
33. Ong, J. N., Jr.; and Fassell, W. M., Jr.: Kinetics of Oxidation of Columbium and Other Refractory Metals. Corrosion, vol. 18, no. 10, Oct. 1962, pp. 382t-389t.

34. Ong, J. N., Jr.; and Fassel, W. M., Jr.: Effects of Alloying Elements on the Oxidation of Refractory Metals. Refractory Metals and Alloys, II. Vol. 17 of Metallurgical Society Conferences. M. Semchyshen and I. Perlmutter, eds., Interscience Publishers, Inc., 1963, pp. 223-268.
35. Simnad, M.; and Smoluchowski, R.: Effect of Proton Irradiation Upon the Electrode Potential of Tungsten. Phys. Rev., vol. 99, no. 6, Sept. 15, 1955, pp. 1891-1892.
36. Spilners, Aija; and Smoluchowski, R.: Effect of Proton Irradiation Upon Catalytic Activity. Reactivity of Solids. J. H. deBoer, ed., D. van Nostrand Co., Inc., 1961, pp. 475-478.
37. Rieman, William; Neuss, Jacob D.; and Naiman, Barnett: Quantitative Analysis. Third ed., McGraw-Hill Book Co., Inc., 1950, pp. 423-425.
38. Breden, C. R.: Light and Heavy Water. Reactor Handbook. Vol. I, Materials. Second ed., C. R. Tipton, Jr., ed., Interscience Publishers, Inc., 1960, pp. 838-887.
39. Primak, W.; and Fuchs, L. H.: Nitrogen Fixation in a Nuclear Reactor. Nucleonics, vol. 13, no. 3, Mar. 1955, pp. 38-41.
40. Stephens, Joseph R.: Effects of Interstitial Impurities on the Low-Temperature Tensile Properties of Tungsten. NASA TN D-2287, 1964.
41. Stephens, Joseph R.: Effect of Oxygen on Mechanical Properties of Tungsten. NASA TN D-1581, 1963.
42. Moteff, J.; and Smith, J. P.: Recovery of Defects in Neutron-Irradiated Tungsten. Symposium on Flow and Fracture of Metals and Alloys in Nuclear Environments. Spec. Tech. Pub. No. 380, ASTM, 1965, pp. 171-187.
43. Jaffee, R. I.; Maykuth, D. J.; and Douglass, R. W.: Rhenium and the Refractory Platinum-Group Metals. Refractory Metals and Alloys. Vol. 11 of Metallurgical Society Conferences. M. Semchyshen and J. J. Harwood, eds., Interscience Publishers, Inc., 1961, pp. 383-463.
44. Aitken, E. A.: Some Comments Regarding Sintering Characteristics in a Radiation Environment. Symposium on Radiation Effects in Refractory Fuel Compounds. Spec. Tech. Pub. No. 306, ASTM, 1962, pp. 123-130.
45. Coble, R. L.; and Burke, J. E.: Sintering in Crystalline Solids. Reactivity of Solids. J. H. de Boer, ed., D. van Nostrand Co., Inc., 1961, pp. 38-51.
46. Van Bueren, H. G.; and Hornstra, J.: Grain Boundaries and the Sintering Mechanism. Reactivity of Solids. J. H. de Boer, ed., D. van Nostrand Co., Inc., 1961, pp. 112-121.

47. Wronski, A. ; and Fourdeux, A. : Slip-Induced Cleavage in Polycrystalline Tungsten. *J. Less-Common Metals*, vol. 6, 1964, pp. 413-429.
48. Wronski, A. ; and Fourdeux, A. : The Ductile-Brittle Transition in Polycrystalline Tungsten. *J. Less-Common Metals*, vol. 8, 1965, pp. 149-158.
49. Ryan, H. F. ; and Suiter, J. : Field Ion Microscope Observations of Stacking Faults in Tungsten. *J. Less-Common Metals*, vol. 9, 1965, pp. 258-262.
50. Ryan, H. F. ; and Suiter, J. : Cavities in Tungsten. *J. Less-Common Metals*, vol. 9, 1965, pp. 307-308.
51. McCoy, H. E. : Creep-Rupture Properties of Tungsten and Tungsten-Base Alloys. Rep. ORNL-3992, Oak Ridge National Lab. , Aug. 1966.
52. McCoy, H. E. , Jr. ; and Steigler, J. O. : Mechanical Behavior of Chemically Vapor Deposited Tungsten at Elevated Temperatures. Rep. ORNL-4162, Oak Ridge National Lab. , Sept. 1967.
53. Wechsler, Monroe S. : Fundamental Aspects of Radiation Effects on Diffusion-Controlled Reactions in Alloys. Symposium on Radiation Effects on Metals and Neutron Dosimetry. Spec. Tech. Pub. No. 341, ASTM, 1963, pp. 86-114.
54. Kinchin, G. H. ; and Thompson, M. W. : Irradiation Damage and Recovery in Molybdenum and Tungsten. *J. Nucl. Energy*, vol. 6, no. 4, pt. I, 1958, pp. 275-284.
55. Thompson, M. W. : The Damage and Recovery of Neutron Irradiated Tungsten. *Phil. Mag. Ser. 8*, vol. 5, no. 51, Mar. 1960, pp. 278-296.
56. Dubrovin, K. P. ; Konobeyevskiy, S. T. ; Levitskiy, B. M. ; Panteleyev, L. D. ; Platonov, P. A. ; and Pravdyuk, N. F. : The Relaxation of Elastic Stress Under Neutron Irradiation. *Properties of Reactor Materials and the Effects of Radiation Damage*. D. J. Littler, ed. , Butterworth and Co. , 1962, pp. 233-244.
57. Bush, Spencer H. : Irradiation Effects in Cladding and Structural Materials. Rowman and Littlefield, Inc. , 1965, pp. 179-205.
58. Muller, Erwin W. : Observations of Radiation Damage With the Field Ion Microscope. *Reactivity of Solids*. J. H. de Boer, ed. , D. van Nostrand Co. , Inc. , 1961, pp. 682-691.
59. Barnes, R. S. : Mechanisms of Radiation-Induced Mechanical Property Changes. Symposium on Flow and Fracture of Metals and Alloys in Nuclear Environments. Spec. Tech. Pub. No. 380, ASTM, 1965, pp. 40-68.
60. Billington, Douglas S. ; and Crawford, James H. , Jr. : *Radiation Damage in Solids*. Princeton University Press, 1961.

61. Anon. : Radiation Effects in Inorganic Solids. Disc. Faraday Soc. , no. 31, 1961.
62. Pearlstein, E. ; Ingham, H. ; and Smoluchowski, R. : Energy Dependence of Radiation Effects in Solids. Phys. Rev. , vol. 98, no. 5, June 1, 1955, p. 1530.
63. Blewitt, T. H. ; Coltman, R. R. ; Holmes, D. K. ; and Noggle, T. S. : Mechanism of Annealing in Neutron Irradiated Metals. J. Appl. Phys. , vol. 28, no. 6, June 1957, pp. 84-110.
64. Muss, D. R. ; and Townsend, J. R. : Energy Dependence of Radiation Damage in Tungsten. J. Appl. Phys. , vol. 32, no. 2, Feb. 1961, pp. 189-192.
65. Gray, D. L. ; and Cummings, W. V. , Jr. : An X-Ray Diffraction Study of Irradiated Molybdenum. Acta Met. , vol. 8, no. 7, July 1960, pp. 446-452.
66. Olson, Paul S. ; Sims, Farrel L. ; and Moteff, John: Neutron Dosimetry Procedures for NMPO Experiments in the ETR. Rep. TM 62-8-28, Nucl. Mat. Prop. Operation, General Electric Co. , Sept. 26, 1962.
67. Ritzman, R. L. ; Lieberman, R. ; Kircher, J. F. ; and Sunderman, D. N. : Fast Neutron Dosimetry for Long-Term Irradiations. Symposium on Radiation Effects on Metals and Neutron Dosimetry. Spec. Tech. Pub. No. 341, ASTM, 1963, pp. 141-150.

TABLE I. - SPECTROGRAPHIC AND CHEMICAL
ANALYSIS OF TUNGSTEN SPECIMENS

Element	Composition, ppm	
	Tensile specimens ^a	Bend specimens ^b
Aluminum	10	3
Boron	^c ND < 2	ND < 2
Carbon	22	15
Calcium	ND < 10	ND < 10
Cobalt	-----	ND < 1
Chromium	ND < 5	ND < 5
Copper	2	ND < 1
Iron	5	7
Potassium	ND < 10	ND < 10
Manganese	ND < 1	ND < 1
Molybdenum	10	10
Sodium	ND < 10	ND < 10
Nickel	5	ND < 2
Oxygen	11	-----
Phosphorous	ND < 20	ND < 20
Lead	ND < 10	ND < 10
Sulfur	ND < 10	18
Silicon	ND < 3	ND < 3
Tin	ND < 5	ND < 5
Thorium	ND < 30	ND < 30
Tungsten	Bal.	Bal.

^a0.500-in. - (12.7-mm-) diameter rod.

^b0.125-in. - (3.2-mm-) diameter rod.

^cND < indicates not detected, less than value given.

TABLE II. - INTEGRATED NEUTRON FLUX
 PROFILES ALONG CENTERLINE OF
 PLUM BROOK REACTOR LATTICE
 POSITION LA-7^a

Irradiation capsule tier ^b number	Distance from reactor core horizontal midplane		Integrated neutron flux, neutrons/cm ²	
	in.	cm		
Top	9.0	22.9	0.7×10 ²⁰	} Thermal
8	5.6	14.3	2.5	
7	2.6	6.7	3.1	
6	-.4	-1.0	3.6	
5	-2.9	-7.3	3.8	
4	-5.4	-13.7	3.6	
3	-7.9	-20.0	3.2	
2	-10.4	-26.4	2.4	
1	-12.9	-32.7	1.7	
Bottom	-15.3	-38.7	.9	
Top	11.0	27.9	1.5×10 ¹⁹	} Fast ^c
8	7.6	19.4	5.5	
7	4.6	11.8	7.9	
6	1.6	4.1	10.7	
5	-1.4	-3.5	10.7	
4	-3.9	-9.8	10.7	
3	-6.4	-16.2	10.1	
2	-8.9	-22.5	8.8	
1	-11.4	-28.9	5.6	
Bottom	-14.3	-36.2	2.2	

^aSee fig. 16.

^bSee fig. 7.

^cNeutron energy greater than 1 MeV.

TABLE III. - TEST SPECIMEN INTEGRATED NEUTRON FLUX^a

Irradiation capsule tier ^b number	Distance from reactor core horizontal midplane		Integrated neutron flux, ^c neutrons/cm ²	
	in.	cm	Fast ^d	Thermal
8	6.6	16.8	6.4×10 ¹⁹	2.0×10 ²⁰
7	3.6	9.1	9.4	3.0
6	.6	1.5	10.6	3.7
5	-2.2	-5.5	10.7	3.8
4	-4.7	-11.7	10.6	3.7
3	-7.2	-18.2	9.7	3.3
2	-9.7	-24.5	7.7	2.7
1	-12.2	-30.9	4.6	1.9

^aSee fig. 16.

^bSee fig. 7.

^cValue on centerline of irradiation capsule (fig. 7, position G), adjacent to center of specimen gage length.

^dNeutron energy greater than 1 MeV.

TABLE IV. - TENSILE PROPERTIES^a OF TUNGSTEN

Specimen number ^b	Irradiation capsule location ^c		Integrated fast ^d neutron flux, neutrons/cm ²	Test temperature		Yield point stress		Ultimate tensile strength		Fracture stress		Reduction of area, percent	Type of fracture ^e
	Tier number	Tier position		°F	K	psi	N/cm ²	psi	N/cm ²	psi	N/cm ²		
T-52	1	A	4.6×10 ¹⁹	Room	Room	(f)	(f)	(f)	(f)	(f)	(f)	(f)	S
T-49	2	A	7.7	↓	↓	↓	↓	↓	↓	↓	↓	↓	S
T-43	4	A	10.6	↓	↓	↓	↓	↓	↓	↓	↓	↓	S
T-42	5	C	10.7	↓	↓	↓	↓	↓	↓	↓	↓	↓	S
T-40	5	A	10.7	↓	↓	↓	↓	↓	↓	↓	↓	↓	S
CT-55	--	--	0	300	422	-----	-----	-----	-----	66.5×10 ³	45.9×10 ³	0	S
CT-56	--	--	0	↓	↓	-----	-----	-----	-----	70.5	48.6	-----	S
CT-60	--	--	0	↓	↓	-----	-----	-----	-----	69.5	47.9	0	S
T-54	1	C	4.6×10 ¹⁹	↓	↓	-----	-----	-----	-----	49.4	34.1	0	D
T-41	5	B	10.7	↓	↓	-----	-----	-----	-----	47.8	33.0	0	D
CT-5	--	--	0	400	477	-----	-----	-----	-----	67.7	46.7	.9	S
CT-6	--	--	0	↓	↓	-----	-----	-----	-----	66.5	45.9	.7	S
CT-58	--	--	0	↓	↓	60.9×10 ³	42.0×10 ³	63.7×10 ³	43.9×10 ³	64.4	44.4	1.1	S
T-44	4	B	10.6×10 ¹⁹	↓	↓	-----	-----	-----	-----	56.5	39.0	0	S
T-45	4	C	10.6	↓	↓	-----	-----	-----	-----	58.3	40.2	0	S
CT-7	--	--	0	500	533	47.7×10 ³	32.9×10 ³	66.5×10 ³	45.9×10 ³	-----	-----	-----	S
CT-8	--	--	0	↓	↓	51.5	35.5	65.5	45.2	67.6×10 ³	46.6×10 ³	3.2	S
CT-9	--	--	0	↓	↓	48.4	33.4	65.0	44.8	69.1	47.6	6.0	S
T-46	3	A	9.7×10 ¹⁹	↓	↓	-----	-----	-----	-----	61.4	42.3	0	S
T-47	3	B	9.7	↓	↓	-----	-----	-----	-----	55.6	38.3	0	S
T-48	3	C	9.7	↓	↓	-----	-----	-----	-----	48.7	33.6	0	S
CT-10	--	--	0	600	589	35.2×10 ³	24.3×10 ³	60.4×10 ³	41.7×10 ³	107.5	74.1	49.3	S
CT-11	--	--	0	↓	↓	39.8	27.4	61.6	42.5	90.0	62.1	33.2	S
CT-12	--	--	0	↓	↓	33.8	23.3	58.9	40.6	86.3	59.5	33.2	S
T-50	2	B	7.7×10 ¹⁹	↓	↓	-----	-----	-----	-----	70.4	48.5	0	D
T-51	2	C	7.7	↓	↓	-----	-----	-----	-----	66.7	46.0	0	S
CT-13	--	--	0	700	644	20.3×10 ³	14.0×10 ³	54.8×10 ³	37.8×10 ³	128.0	88.3	67.7	S
CT-15	--	--	0	↓	↓	21.9	15.1	55.1	38.0	125.3	86.4	67.7	S
CT-59	--	--	0	↓	↓	22.4	15.4	56.0	38.6	134.0	92.4	67.7	S
T-53	1	B	4.6×10 ¹⁹	↓	↓	-----	-----	-----	-----	37.1	25.6	0	S

^aSee fig. 17.

^bCT-XX indicates unirradiated (control) tungsten tensile specimen; T-XX indicates irradiated tungsten tensile specimen.

^cSee fig. 7.

^dSee table III.

^eS indicates single fracture; D indicates double fracture.

^fSpecimen fractured in handling after irradiation.

TABLE V. - EXTREME FIBER STRESS^a OF TUNGSTEN

Specimen number ^b	Surface finish	Irradiation capsule location ^c		Integrated fast ^d neutron flux, neutrons/cm ²	Extreme fiber stress	
		Tier number	Tier position		psi	N/cm ²
C-116-T	Unpolished ↓	--	--	0	138.3×10 ³	95.2×10 ³
C-117-T		--	--	0	141.0	97.2
C-118-T		--	--	0	147.4	101.6
89-T		7	D	9.4×10 ¹⁹	92.3	63.6
90-T		7	E	9.4	87.1	60.1
91-T		7	F	9.4	103.2	71.2
C-61-T	Polished ↓	--	--	0	154.0×10 ³	106.2×10 ³
C-62-T		--	--	0	154.0	106.2
C-63-T		--	--	0	151.0	104.1
7-T		8	D	6.4×10 ¹⁹	113.5	78.3
8-T		8	E	6.4	90.2	62.2
9-T		8	F	6.4	114.7	79.1
10-T		6	D	10.6	92.6	63.9
11-T		6	E	10.6	93.2	64.3
12-T		6	F	10.6	99.9	68.9

^aSee fig. 21.

^bC-XXX-T indicates unirradiated (control) tungsten bend specimen; XX-T indicates irradiated tungsten bend specimen.

^cSee fig. 7.

^dSee table III.

TABLE VI. - CHANGE IN TUNGSTEN TEST SPECIMEN DIMENSIONS^a

Specimen number ^b	Irradiation capsule location ^c		Integrated fast ^d neutron flux, neutrons/cm ²	Length				Length change, $\Delta L/L$, percent	Diameter				Diameter change, $\Delta D/D$, percent
	Tier number	Tier position		in.		mm			in.		mm		
				Pre-irradiation	Change	Pre-irradiation	Change		Pre-irradiation	Change	Pre-irradiation	Change	
T-52	1	A	4.6×10 ¹⁹	2.50590	0.00081	63.64986	0.02057	0.032	0.18992	-0.00082	4.82397	-0.02083	-0.43
T-53	1	B	4.6	2.50101	.00034	63.52565	.00864	.014	.19027	-.00047	4.83286	-.01194	-.25
T-54	1	C	4.6	2.50515	.00093	63.63081	.02362	.037	.18983	-.00088	4.82168	-.02235	-.46
7-T	8	D	6.4	2.86732	.00189	72.82993	.04801	.066	.11488	.00012	2.91795	.00305	.10
8-T	8	E	6.4	2.86787	.00148	72.84390	.03759	.052	.11460	.00014	2.91084	.00356	.12
9-T	8	F	6.4	2.86715	.00110	72.82561	.02794	.038	.11472	.00023	2.91389	.00584	.20
T-49	2	A	7.7	2.50503	.00125	63.62776	.03175	.050	.19012	-.00112	4.82905	-.02845	-.59
T-50	2	B	7.7	2.49622	.00085	63.40399	.02159	.034	.19018	-.00041	4.83057	-.01041	-.22
T-51	2	C	7.7	2.50023	.00122	63.50584	.03099	.049	.19003	-.00098	4.82676	-.02489	-.52
89-T	7	D	9.4	2.88067	.00141	73.16902	.03581	.049	.12513	.00020	3.17830	.00508	.16
90-T	7	E	9.4	2.87841	.00119	73.11161	.03023	.041	.12540	.00015	3.18516	.00381	.12
91-T	7	F	9.4	2.87982	.00112	73.14743	.02845	.039	.12531	-.00011	3.18287	-.00279	-.09
T-46	3	A	9.7	2.50014	.00129	63.50356	.03277	.052	.18990	-.00109	4.82346	-.02769	-.57
T-47	3	B	9.7	2.49951	.00089	63.48755	.02261	.036	.18954	-.00063	4.81432	-.01600	-.33
T-48	3	C	9.7	2.50284	.00105	63.57214	.02687	.042	.18976	-.00098	4.81990	-.02489	-.52
T-43	4	A	10.6	2.49937	.00134	63.48400	.03404	.054	.19011	-.00056	4.82879	-.01422	-.29
T-44	4	B		2.50266	.00205	63.56756	.05207	.082	.18978	-.00071	4.82041	-.01803	-.37
T-45	4	C		2.50164	.00136	63.54166	.03454	.054	.19019	-.00124	4.83083	-.03150	-.65
10-T	6	D		2.86475	.00154	72.76465	.03912	.054	.11497	-.00041	2.92024	-.01041	-.36
11-T	6	E		2.86358	.00163	72.73493	.04140	.057	.11482	.00028	2.91643	.00711	.24
12-T	6	F		2.86395	.00172	72.74433	.04369	.060	.11398	-.00011	2.89509	-.00279	-.10
T-40	5	A	10.7	2.50237	-----	63.56020	-----	-----	.19004	-----	4.82702	-----	-----
T-41	5	B	10.7	2.50203	0.00103	63.55156	0.02616	0.041	.18996	-0.00046	4.82498	-0.01168	-0.24
T-42	5	C	10.7	2.50033	.00102	63.50838	.02591	.041	.19006	-.00056	4.82752	-.01422	-.29

^aAll measurements made at room temperature; see fig. 23.

^bT-XX indicates irradiated tungsten tensile specimen; XX-T indicates irradiated tungsten bend specimen.

^cSee fig. 7.

^dSee table III.

TABLE VII. - CHANGES IN TUNGSTEN TEST SPECIMEN DENSITY, WEIGHT, AND VOLUME^a

Specimen number ^b	Irradiation capsule location ^c		Integrated neutron flux, fast ^d neutrons/cm ²	Density at 68° F (293 K), g/cm ³		Weight in air, g		Volume, cm ³			
	Tier number	Tier position		Pre-irradiation	Change	Pre-irradiation	Change	Pre-irradiation ^e	Post-irradiation change ^f	Specific weight loss change ^g	Corrected change ^h
T-52	1	A	4.6×10 ¹⁹	19.2231	-0.3274	74.4490	-0.3425	3.8729	0.0490	0.0178	0.0668
T-53	1	B	4.6	-----	-----	74.2893	-.2759	-----	-----	-----	-----
T-54	1	C	4.6	-----	-----	75.8360	-.3834	-----	-----	-----	-----
7-T	8	D	6.4	19.1915	-0.1318	9.3536	-0.0349	0.4874	0.0015	0.0018	0.0033
8-T	8	E	6.4	19.1812	-.1167	9.2563	-.0424	.4826	.0007	.0022	.0029
9-T	8	F	6.4	19.1690	-.1220	9.2600	-.0353	.4831	.0012	.0018	.0030
T-49	2	A	7.7	19.2490	-.1064	74.2563	-.3724	3.8577	.0020	.0193	.0213
T-50	2	B	7.7	19.2401	-.0759	73.7262	-.3270	3.8319	-.0019	.0170	.0151
T-51	2	C	7.7	19.2381	-.0422	74.2756	-.3801	3.8609	-.0114	.0198	.0084
89-T	7	D	9.4	19.2399	-.0668	11.2071	-.0647	.5825	-.0014	.0034	.0020
90-T	7	E	9.4	19.2533	-.0803	11.1898	-.0601	.5812	-.0007	.0031	.0024
91-T	7	F	9.4	19.2281	-.1238	11.2137	-.0623	.5832	.0005	.0032	.0037
T-46	3	A	9.7	19.2392	-.0561	74.2553	-.4792	3.8596	-.0137	.0249	.0112
T-47	3	B	9.7	19.2362	-.0322	74.1451	-.3451	3.8545	-.0116	.0179	.0063
T-48	3	C	9.7	19.2330	-.0148	74.1578	-.4034	3.8558	-.0181	.0210	.0029
T-43	4	A	10.6	19.2354	-.1783	73.8507	-.4827	3.8393	.0142	.0251	.0393
T-44	4	B		19.2423	-.1420	73.8214	-.3463	3.8364	-.0180	.0180	0
T-45	4	C		19.2294	-.0904	74.1305	-.4330	3.8551	-.0045	.0225	.0180
10-T	6	D		19.1826	.2682	9.2685	-.0702	.4832	-.0103	.0037	-.0066
11-T	6	E		19.2823	.0268	9.2761	-.0450	.4811	-.0030	.0023	-.0007
12-T	6	F		19.1794	.2080	9.1584	-.0524	.4775	-.0078	.0027	-.0051
T-40	5	A	10.7	19.2346	-----	74.4394	-----	-----	-----	-----	-----
T-41	5	B	10.7	19.2419	-0.0704	74.3559	-0.3481	3.8643	-0.0040	0.0181	0.0141
T-42	5	C	10.7	19.2411	-----	74.4995	-----	-----	-----	-----	-----

^aSee figs. 24 and 25.

^bT-XX indicates irradiated tungsten tensile specimen; XX-T indicates irradiated tungsten bend specimen.

^cSee fig. 7.

^dSee table III.

^ePreirradiation weight in air divided by preirradiation density.

^fPreirradiation weight in air divided by preirradiation density minus postirradiation weight in air divided by postirradiation density.

^gPreirradiation weight in air minus postirradiation weight in air divided by preirradiation density.

^hMeasured change in volume plus weight loss change in volume.

TABLE VIII. - ELECTRICAL RESISTIVITY OF TUNGSTEN^a

Specimen number ^b	Irradiation capsule location ^c		Integrated neutron flux, neutrons/cm ²		Electrical resistivity at 100° F (311 K), ohm-cm	(Electrical resistivity)/Density, (ohm-cm ⁴)/g		
	Tier number	Tier position	Fast ^d	Thermal		Control	Postirradiation	Change
CT-5	--	--	0	0	5.784×10 ⁻⁶	0.301×10 ⁻⁶	-----	-----
CT-6	--	--	↓	↓	5.802	-----	-----	-----
CT-7	--	--	↓	↓	5.833	0.304×10 ⁻⁶	-----	-----
CT-8	--	--	↓	↓	5.799	.302	-----	-----
CT-9	--	--	↓	↓	5.884	.307	-----	-----
CT-10	--	--	↓	↓	5.872	.305	-----	-----
CT-11	--	--	↓	↓	5.863	.305	-----	-----
CT-12	--	--	↓	↓	5.815	.302	-----	-----
CT-13	--	--	↓	↓	5.830	.303	-----	-----
CT-15	--	--	↓	↓	5.858	.305	-----	-----
CT-55	--	--	↓	↓	5.809	.302	-----	-----
CT-56	--	--	↓	↓	5.804	.302	-----	-----
CT-57	--	--	↓	↓	5.844	.304	-----	-----
CT-58	--	--	↓	↓	5.895	.307	-----	-----
C-61-T	--	--	↓	↓	5.888	.306	-----	-----
C-62-T	--	--	↓	↓	5.879	.306	-----	-----
C-63-T	--	--	↓	↓	5.869	.305	-----	-----
C-116-T	--	--	↓	↓	5.846	.305	-----	-----
C-117-T	--	--	↓	↓	5.923	.309	-----	-----
C-118-T	--	--	↓	↓	5.784	.301	-----	-----
T-52	1	A	4.6×10 ¹⁹	1.9×10 ²⁰	9.275	.304	0.491×10 ⁻⁶	0.187×10 ⁻⁶
T-53	1	B	4.6	1.9	8.836	.304	.460	.156
T-54	1	C	4.6	1.9	9.333	-----	-----	-----
7-T	8	D	6.4	2.0	10.051	0.304×10 ⁻⁶	0.527×10 ⁻⁶	0.223×10 ⁻⁶
8-T	8	E	6.4	2.0	9.767	↓	.512	.208
9-T	8	F	6.4	2.0	9.879	↓	.519	.215
T-49	2	A	7.7	2.7	10.123	↓	.529	.225
T-50	2	B	7.7	2.7	9.702	↓	.506	.202
T-51	2	C	7.7	2.7	10.111	↓	.527	.223
89-T	7	D	9.4	3.0	10.503	↓	.548	.244
90-T	7	E	9.4	3.0	10.337	↓	.539	.235
91-T	7	F	9.4	3.0	10.346	↓	.542	.238
T-46	3	A	9.7	3.3	10.574	↓	.551	.247
T-47	3	B	9.7	3.3	10.268	↓	.535	.231
T-48	3	C	9.7	3.3	10.536	↓	.548	.244
T-43	4	A	10.6	3.7	10.926	↓	.573	.269
T-44	4	B	↓	↓	10.428	↓	.546	.242
T-45	4	C	↓	↓	10.806	↓	.565	.261
10-T	6	D	↓	↓	10.887	↓	.560	.256
11-T	6	E	↓	↓	10.784	↓	.558	.254
12-T	6	F	↓	↓	10.835	↓	.559	.255
T-40	5	A	10.7	3.8	-----	-----	-----	-----
T-41	5	B	10.7	3.8	10.445×10 ⁻⁶	0.304×10 ⁻⁶	0.545×10 ⁻⁶	0.241×10 ⁻⁶
T-42	5	C	10.7	3.8	-----	-----	-----	-----

^aSee figs. 26 and 27.

^bCT-XX indicates unirradiated (control) tungsten tensile specimen; C-XXX-T indicates unirradiated (control) tungsten bend specimen; T-XX indicates irradiated tungsten tensile specimen; and XX-T indicates irradiated tungsten bend specimen.

^cSee fig. 7.

^dSee table III.

FIRST CLASS MAIL

030 001 42 51 305 68168 00903
AIR FORCE WEAPONS LABORATORY/AFWL/
KILLGORE AIR FORCE BASE, NEW MEXICO 8711

RECEIVED 10 15 1958
MAIL ROOM

POSTMASTER: If Undeliverable (Section 158
Postal Manual) Do Not Return

"The aeronautical and space activities of the United States shall be conducted so as to contribute . . . to the expansion of human knowledge of phenomena in the atmosphere and space. The Administration shall provide for the widest practicable and appropriate dissemination of information concerning its activities and the results thereof."

— NATIONAL AERONAUTICS AND SPACE ACT OF 1958

NASA SCIENTIFIC AND TECHNICAL PUBLICATIONS

TECHNICAL REPORTS: Scientific and technical information considered important, complete, and a lasting contribution to existing knowledge.

TECHNICAL NOTES: Information less broad in scope but nevertheless of importance as a contribution to existing knowledge.

TECHNICAL MEMORANDUMS: Information receiving limited distribution because of preliminary data, security classification, or other reasons.

CONTRACTOR REPORTS: Scientific and technical information generated under a NASA contract or grant and considered an important contribution to existing knowledge.

TECHNICAL TRANSLATIONS: Information published in a foreign language considered to merit NASA distribution in English.

SPECIAL PUBLICATIONS: Information derived from or of value to NASA activities. Publications include conference proceedings, monographs, data compilations, handbooks, sourcebooks, and special bibliographies.

TECHNOLOGY UTILIZATION PUBLICATIONS: Information on technology used by NASA that may be of particular interest in commercial and other non-aerospace applications. Publications include Tech Briefs, Technology Utilization Reports and Notes, and Technology Surveys.

Details on the availability of these publications may be obtained from:

SCIENTIFIC AND TECHNICAL INFORMATION DIVISION
NATIONAL AERONAUTICS AND SPACE ADMINISTRATION
Washington, D.C. 20546